FLOODSTAND
FP7-RTD- 218532

Integrated Flooding Control and Standard for Stability and Crises Management

FLOODSTAND-deliverable:

Numerical study on the critical pressure heads

Authors	Hendrik Naar and Sander Vaher
Organisation	MEC Insenerilahendused
Revision	2.0
Deliverable No.	D2.2a
Date	25 October 2010

Document identification sheet		
FLOODSTAND	**Integrated Flooding Control and Standard for Stability and Crises Management**	FP7-RTD- 218532

Title: Numerical studies and analysis of leaking and collapsing structures	**Other report identifications:**
Investigating partners: MEC **Authors:** Hendrik Naar and Sander Vaher **Reviewed by**:	
[ ] **Outline** [ ] **Draft** [x] **Final** **Version number:** 2.0 **Revision date**: 25 October 2010 **Next version due:** **Number of pages**: 53	[x] **A deliverable** [ ] **Part of a deliverable** [ ] **Cover document for a part of a deliverable** [ ] **Deliverable cover document** [ ] **Other** **Deliverable number**: D2.2a **Work Package**: WP2 **Deliverable due at month**: 17
Accessibility: [x] **Public** [ ] **Restricted** [ ] **Confidential (consortium only)** [ ] **Internal (accessibility defined for the final version)**	**Available from**: http:/floodstand.tkk.fi **Distributed to**: **Disclosees when restricted:** **Comments:**

Abstract: Numerical studies and analysis of leaking and collapsing of structures consisted of two main parts – modelling and results comparison with real scale tests. Modelling was carried out by MEC and tests mainly by CTO. Four main structure types were under study – cold-room, SWT-door, A-60 hinged door and cabin room.

Numerical modelling provided relatively accurate or slightly inordinate critical pressure heads of studied structures, if decent drawings and material properties/test specimens were available. Leakage rate estimation with structural numerical analyse basically failed because a small water passages between structure layers are impossible to see.

Acknowledgements
The research leading to these results has received funding from the European Union's Seventh Framework Programme (FP7/2007-2013) under grant agreement n° 218532. The financial support is gratefully appreciated.

Disclaimer

1. EXECUTIVE SUMMARY

This document is the deliverable of Task 2.2a

Objectives of task T2.2a

Objectives of the task T2.2a is to: obtaining results of numerical analyses of leaking and collapsing structures (partitions) and development of easy-to-use criteria for the partitions in flooding simulation. Also it was important to obtain understanding about the modelling requirements of partitions and door structures in order to estimate properly structural collapse under water pressure.

Summary of task T2.2a

The present report presents numerical studies where the standard doors and lightweight walls are subjected to hydrostatic pressure. The aim was to estimate the collapse pressure for named structures and understand their behaviour. This knowledge helps to develop simplified formulas for collapse pressure estimation that can be used later on in flooding simulation.

Four types of structures were studied: cold-room structure (including wall and door), cabin wall, A-60 hinged door and A-60 semi-watertight sliding door. All these structures were analysed with non-linear finite element method. As a result, the collapse pressure was determined. The study included also determination of material mechanical properties through testing. In order to validate the finite element results full-scale laboratory test were carried out on cold-room and cabin wall panels.

For cold room panel and for cabin wall panel the analytical models where developed in order to estimate the critical pressure heads. For standard door solutions the use of analytical methods is not practical as door failure often depends rather on the strength of joints (like screws, rivets, supporting profiles) as on the strength of the door itself. As a result of analyses critical pressure heads for above mentioned partitions were determined.

In all cases the critical pressure heads are well estimated as they coincide with the tests performed in CTO. The cold room panel sustains approximately 2.7 m of water pressure. A-60 SWT sliding door will collapse at water height 8.1 m where CTO tests indicated collapse at 8.36 m of water height. According to simulation A-60 door will collapse at approximately 2 m of water level due to deformation of door joints. However, in tests CTO pointed out that the leakage limit was reached at 1 m of water level. Tests conducted in MEC and simulation on single cabin wall panel indicates that the panel will fail due to bending already at 1.1 m of water level. However, the panel will not collapse at that point as at the membrane forces start carry the load. Therefore, the final failure occurs at point where the total shear force reaches to value equal to the shear strength of the panel-deck connection. According to CTO the cabin wall panel can carry the load up to 1.2-1.4 m of water level.

.

CONTENTS

Page

2. INTRODUCTION

Different damages of ship hull lead quite often to flooding, which is one of the major risks on passengers' safety. Decisions of actions following to the damage are mainly based on flooding simulations. In current simulations, the affect of non-watertight structures are usually neglected. In real case scenario, some of watertight compartment internal structures can stand quite high pressure and for reliable flooding simulations, the strength of the structures should be taken into account.

The numerical study of every flooding obstacle is unpractical because the non-watertight structures in ship vary in large scale in terms of dimensions as well as in material properties. Due previously named reasons, structures that are subject of certain guidelines or are standard in many passenger ships were selected for numerical and analytical studies. Four main types of structures were under study – cold room walls, cabin walls, A-60 semi-watertight sliding door and A-60 hinged door.

Ship's cold room is a structure on board, which is made of 1200 wide and about 2000mm high polyurethane (PU) sandwich panels. A panel consist of two faceplates and a core between them. The faceplates are made of 0.6...0.8mm thick mild steel sheets and stainless-steel sheets or a combination of these – a galvanized mild steel on outside and a stainless steel on inside. The core plate is about 99mm in thickness and made of polyurethane foam, which provides the thermal insulation and carries force from one face-sheet to another.

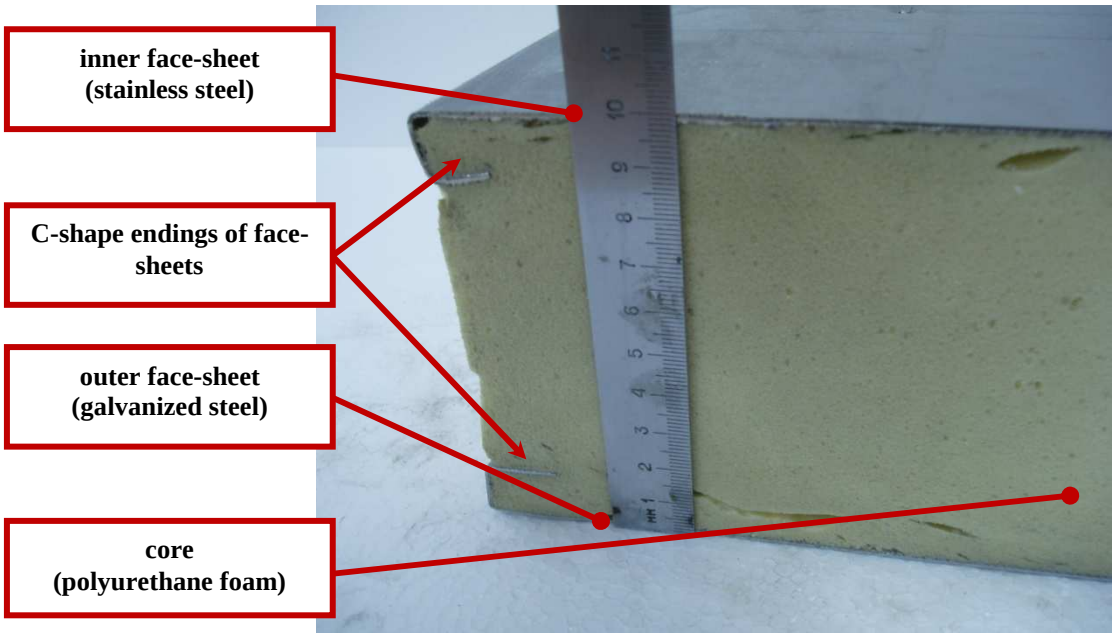

Figure 2.1 Cross-section of a sandwich panel

Two types of fire-doors were selected for studies due to their wide use in ship applications. In both cases, the door-leaf consists of two mild steel plates and a thermal insulation between them. In the

sandwich construction, the core acted as shear stresses carrying element, while in fire-doors the strength is based on steel and the thermal insulation on mineral wool. Two door types differed from each other mainly by thickness of door-leaf steel plates (sliding door is considered as semi-watertight door) and connections to a bulkhead.

Passenger ship cabin-wall construction varies slightly depending on adjacent structures. The studied wall fragment consisted of PVC coated panels with dimensions of 1200mm (width) x 2000mm (height). Panel is constructed of two steel plates and a rigid mineral wool plate. The corrugated sheet (0.4mm) is glued to PVC coated flat sheet (0.6mm), which make the inner surface of the cabin. A 10mm to 20mm (depending on surrounding structures) thick rigid mineral wool plate is glued on outer surface of corrugated sheet to provide a sufficient soundproofing. However, in strength estimation the wool is neglected due imaginary affect.

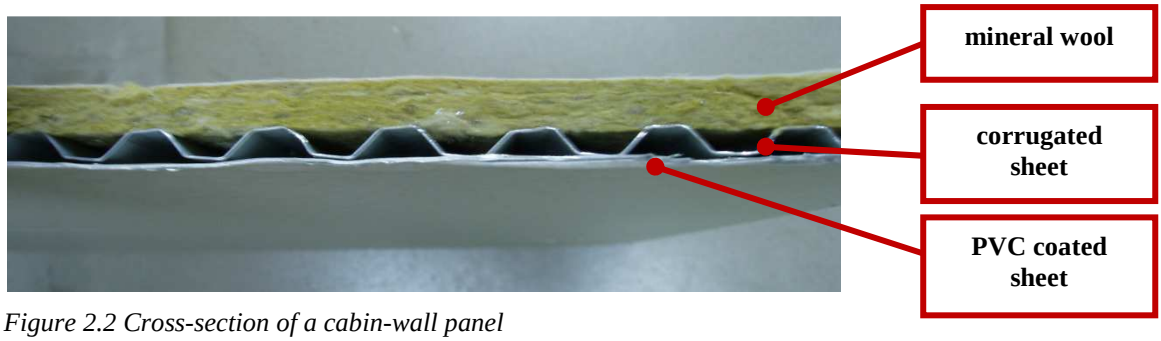

Figure 2.2 Cross-section of a cabin-wall panel

3. TESTS AND SIMULATIONS OF COLD ROOM PANELS

Bending tests, as most appropriate test for estimating the ultimate strength of a panel, were carried out for panels with different spans. It was observed that short span panels (concentrated loading) failed in a just locally, while long span panels failed due the loss of stability in compressed plate (due wrinkling).

In all panel testing midpoint deformation and loading force were digitally saved and a corresponding curve produced.

The stiffness (rising angle of a curve) and ultimate carrying load as the most important parameters of panels can be read from the force-deformation curve.

3.1 Laboratory tests for determination of material properties

The first stage of strength estimation of cold room structure was the determination of single material mechanical properties in laboratory tests. Four tests of each material (mild steel, stainless steel and polyurethane foam (PU-foam)) were accomplished on Zwick/Roell Z250/2.5 testing apparatus and digital output of the results saved. As the stainless steel and normal steel test results were in close relation to material properties described in literature, no further numerical modelling of these materials were carried out. PU-foam compression test had to be modelled in finite element method based program, LS-DYNA, to find out the correlative material from software materials database.

3.1.1 Tensile tests for face materials

Four material examples were extracted from both sides of the sandwich panel. Fragments of sheets were cut into bone shape (20mm wide in strain area) flat specimens and tested under tension until failure. Results were presented in strain-stress curves whereby engineering strain was transferred to

true strain (following graphs represent true strain).

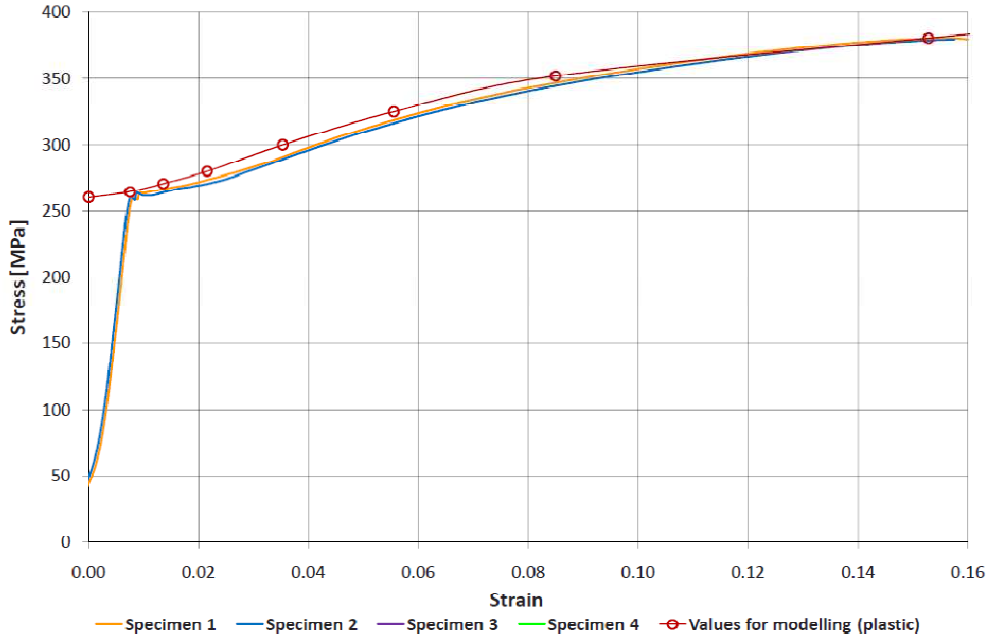

Figure 3.1 Stress-strain curve of mild steel tensile test

The ultimate stress values were calculated by taking into account the dimensions of the necking, which formed during the failure of the specimen. Generated data was used to define material properties for numerical modelling. Face sheet materials testing results had minimal variation as seen in figures 3.1 and 3.2, thus no additional testing was carried out.

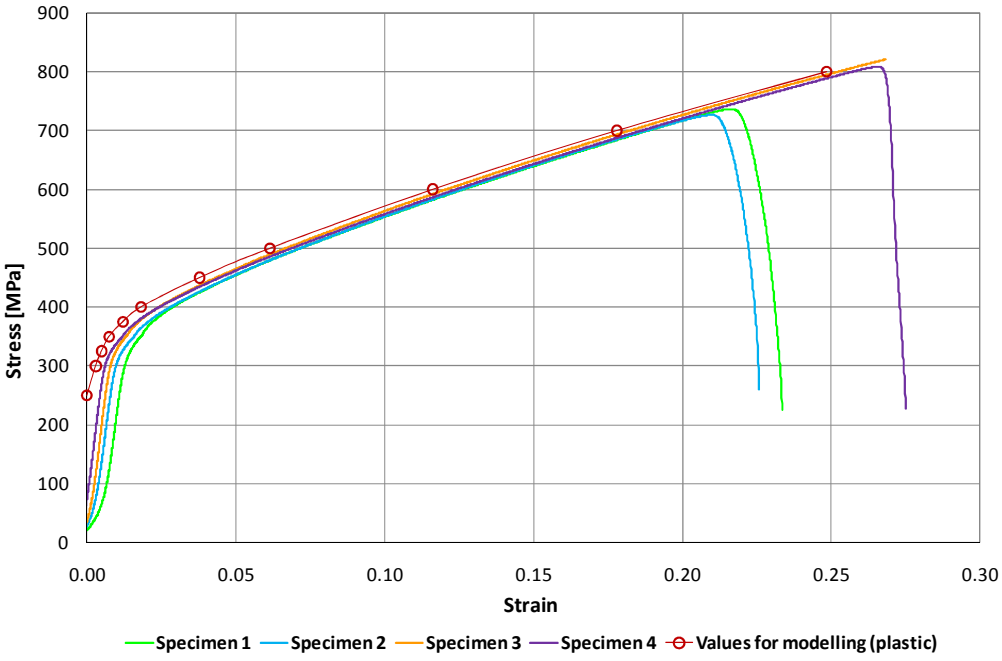

Figure 3.2 Stress-strain curve of stainless steel tensile test

In the numerical model "piecewise linear plasticity" (MAT 24) was used in LS-Dyna code, for modelling the steel materials. Material describing stress-plastic strain curves is shown in figures 3.1 and 3.2. From the curves, it is easy to see that yielding of mild steel started at 260 MPa exactly, while the stainless steel turned from elastic state to plastic quite smoothly. Rest of the required steel material properties were mainly determined according to literature and datasheets of materials.

- Density – 7850 kg/m^3
- Young's modulus – 210 000 MPa
- Plastic stress-strain curve from laboratory test results (figure 3.1 an 3.2)
- Poisson's ratio – 0.3

3.1.2 Compression tests of foam material

PU-foam material compression tests were carried out on Zwick/Roell Z2.5 testing apparatus mainly on 50x50x50mm specimens. Digital results were saved and examined in form of strain-stress curves.

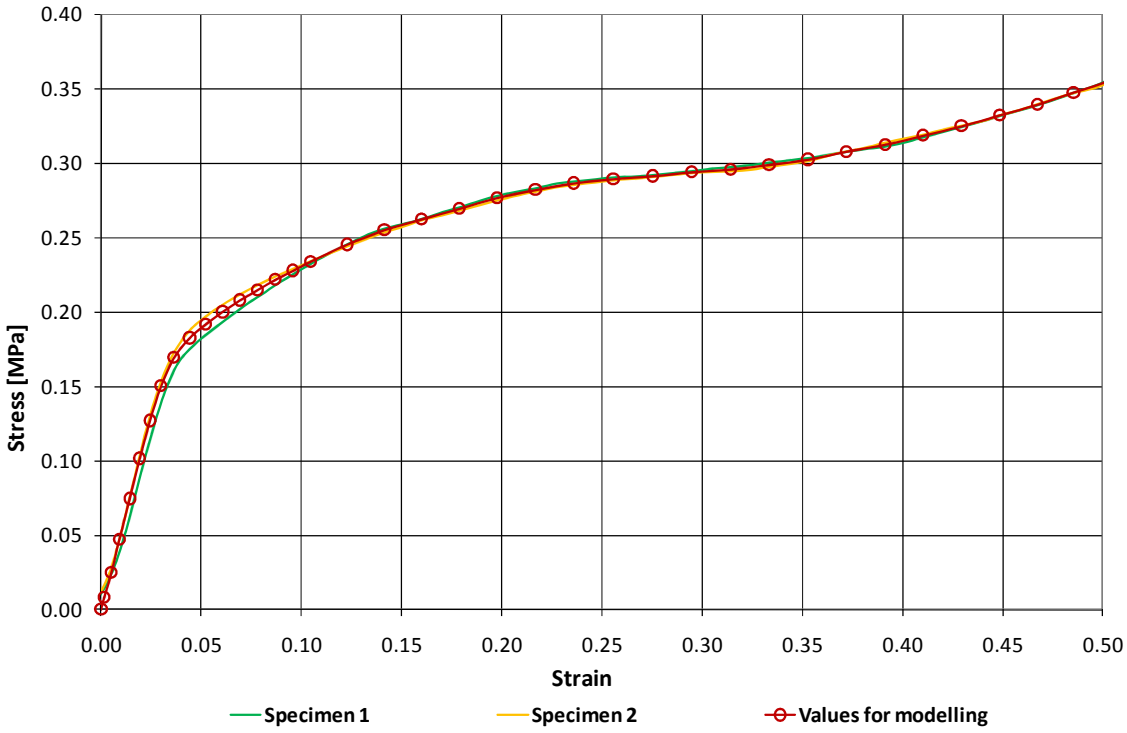

Figure 3.3 Stress-strain curve of polyurethane foam compression test

Results of hot wire cut specimens were removed and two normal specimen's results were presented in figure 3.3.

3.1.3 Tension tests of foam material

In LS-Dyna numerical model, material type LOW_DENSITY_FOAM requires besides compression stress-strain curve also tension Young's modulus. For obtaining a reliable E-value, several specimens were examined besides compression tests also in tension.

PU-foam material tensile tests were carried out on Zwick/Roell Z250 testing apparatus with video extensometer on bone-shape specimens with cross-section 38...39x22...23.5mm. Digital results were saved and examined in strain-stress curves.
Results of tension tests varied in much larger scale compared to compression tests. This phenomena is also recognised among other foam type materials as in compression local failures of material do not affect the results that significantly as in the tension test.

Another key factor regarding foam tests was that Young's modulus in tension was about three times higher compared to compression test. In compression E = 5.3MPa, while in tension E = 15.7MPa. Such behaviour of foam materials is quite well known and can be described referring to the nature of a foam structure. In compression "bubble" walls loose stability in very early stage of loading, while in tension walls act as membrane structure and can resist relatively high stress compared to deformations.

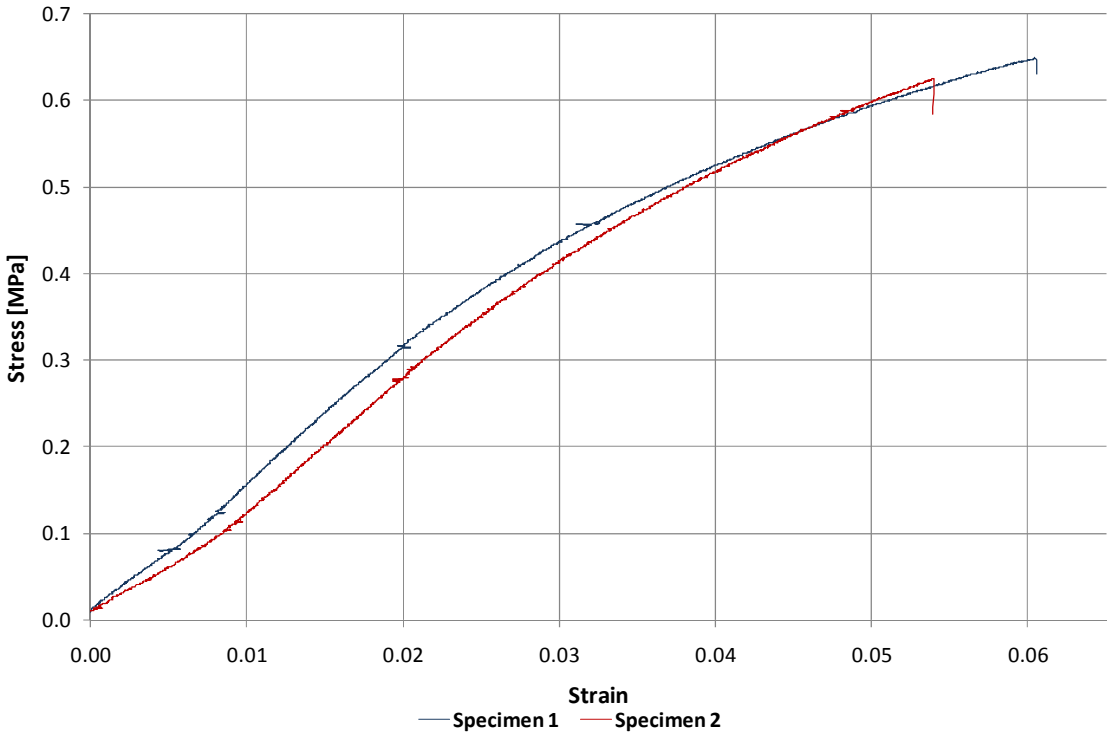

Figure 3.4 Stress-strain curve of PU-foam tension test

3.2 Numerical simulation of foam material

3.2.1 Numerical simulation of foam material compression test

As PU-foam material properties may vary in a large scale and LS-DYNA

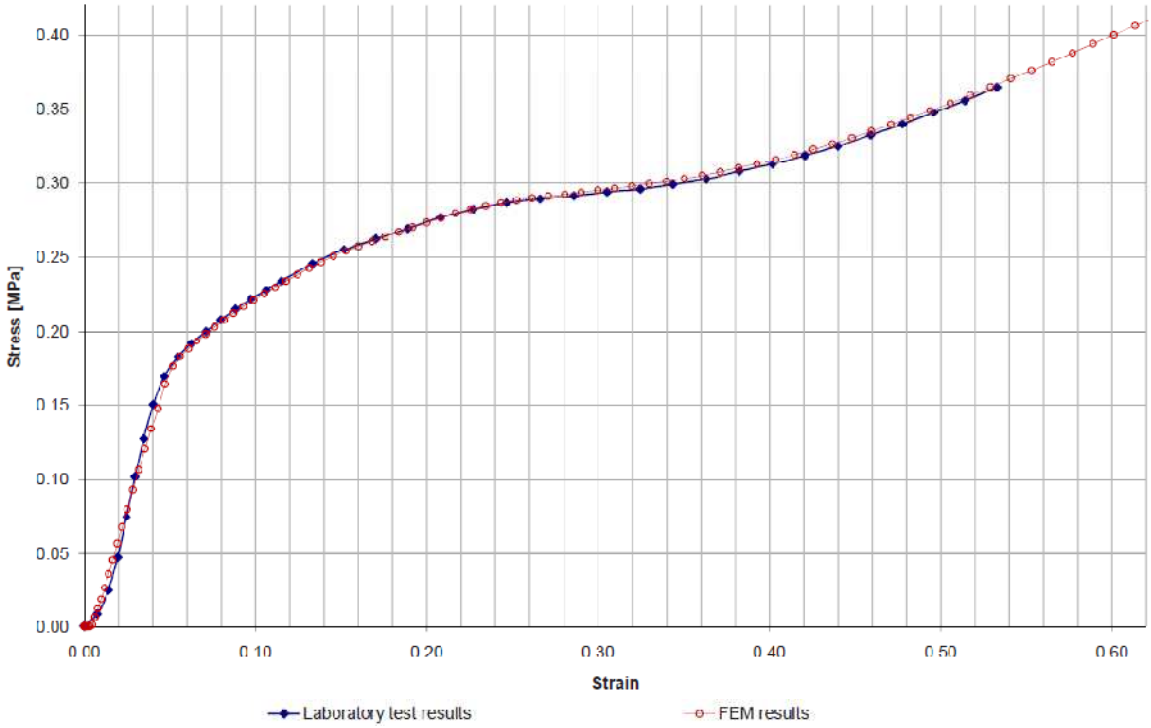

Figure 3.5 PU-foam compression test numerical simulation and laboratory test comparison

provides many different foam material types, laboratory-test-like numerical simulations of compression were carried out to find the most correlative material from LS-DYNA database. Three material types were tested to find the best fitting material for describing the polyurethane foam – LOW_DENSITY_FOAM, CLOSED_CELL_FOAM and CRUSHABLE_FOAM.
As a result of numerical simulation it was concluded that LOW_DENSITY_FOAM had the best correlation with real test results. The parameters used for describing the foam were:

- Density – 52kg/m^3
- Tensile Young's modulus – 15.7 MPa
- Compression Young's modulus – 5.3 MPa
- Compression stress-strain curve from laboratory test results (figure 3.5)
- Tension cut-off stress – 0.62 MPa

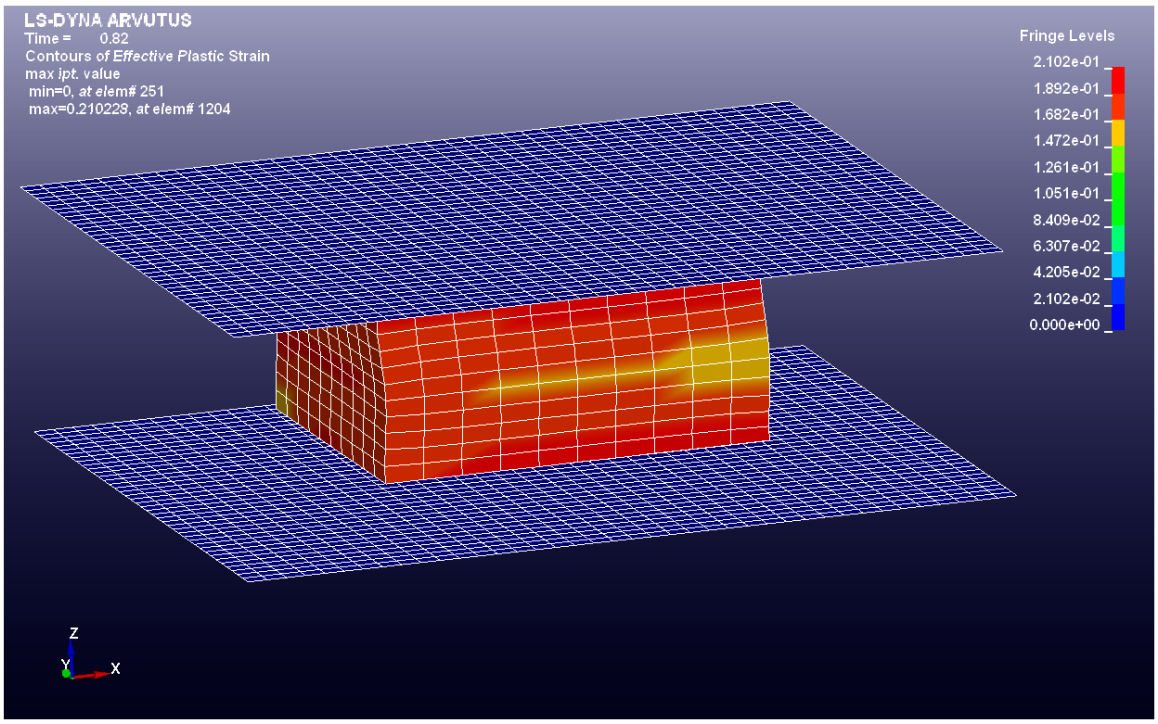

Figure 3.6 Capture of foam cube compression numerical simulation (von Mises stress)

It must be added that the friction factor between foam (specimen) and steel (compression plates) had quite large effect on test results, but overall, the LOW_DENSITY_FOAM was the best for describing PU-foam.

3.3 Bending tests and simulations of sandwich beam

3.3.1 Bending tests and simulation of sandwich beam, with a span 350mm

Bending test of 350mm span panel was carried out on Zwick/Roell Z250 testing machine and results were saved digitally. A deformation–loading force curve was produced to compare the results of numerical simulation of same test.

The panel failed in local mean exactly under the loading point. As such type of failure is not very likely to happen in two-meter high sandwich panel applied with hydrostatic loading, the results could be used just for confirming the chosen material parameters and element sizes for numerical model.
An ultimate bending momentum was not found because there was not certain point when the panel failed. The results in terms of force-deformation curve can be seen in figure 3.8.

Modelling the bending test, previously found material properties were used. Results were closely correlative in first (elastic deformations) phase (no local deformation phase) of the testing, but numerical model was relatively weaker to carry loads in second phase (plastic deformations) of the

testing – local failure phase. In view of the complexity of many simultaneous nonlinear processes in test, numerical modelling results are rather satisfying.

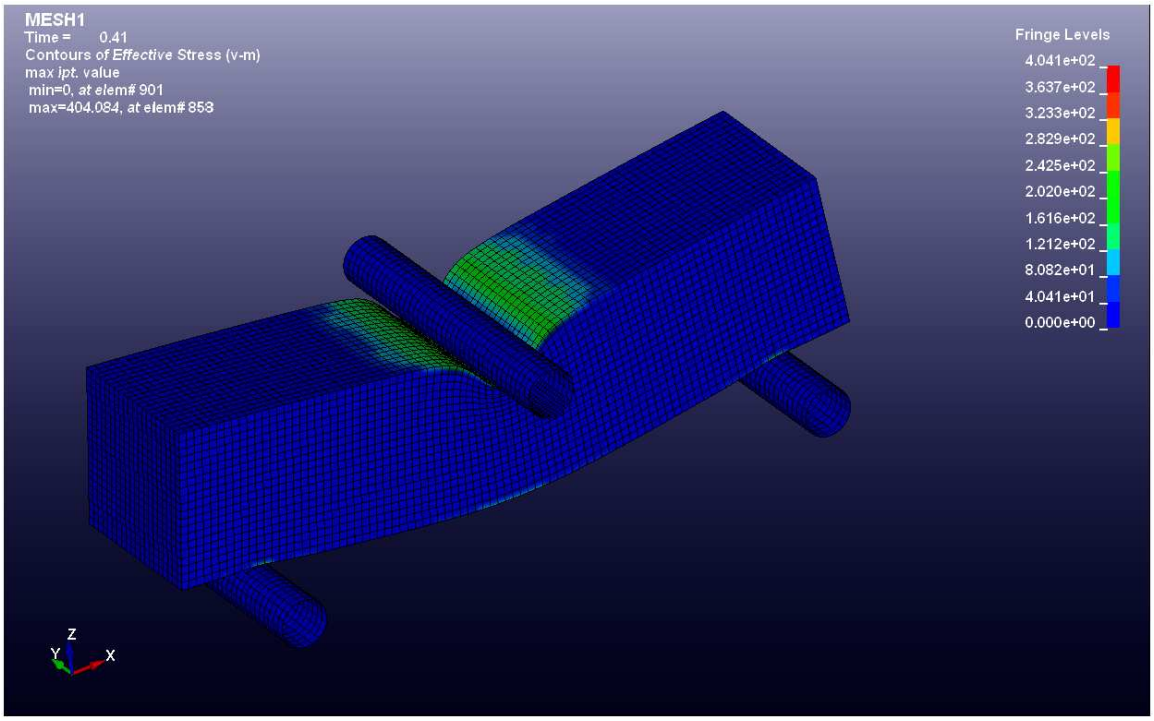

Figure 3.7: Numerical modelling of the short span beam bending (von Mises stress)

Imitating the local failure in FEM model is rather difficult to achieve as the ductile and elastic deformations are occurring in the same time in global as well in local mean.

Nevertheless, the ultimate load carrying capacity was just less than 5% different from the laboratory testing and the rising angle of stiffness curve were basically identical. Such behaviour is most probably caused by the specific properties, used for describing the foam material. Mat_057 requires just compression stress-strain curve, while tension characterized by just two values – Young's modulus and tension cut-off stress.

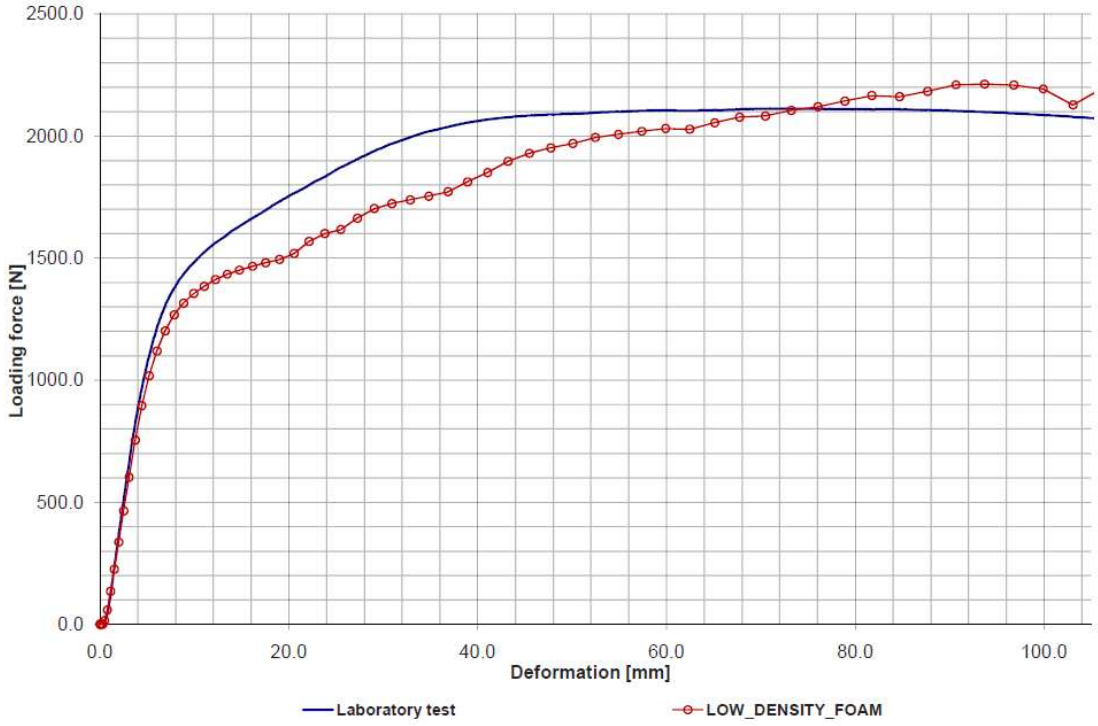

Figure 3.8: Results of short span bending test

3.3.2 Bending tests and simulation of sandwich beam, with a span 1800mm

The test was carried out on especially for Floodstand project designed bending frame (see Appendixes). A distributed load is achieved by six simultaneously working hydraulic cylinders that were subject to equal oil pressure. A digital output of oil pressure and deflection of a specimen were saved.

Oil pressure values were transferred to force of hydraulic cylinders according to calibration. Two similar calibrations were performed – first with a known rectangular hollow steel beam with a strain gauge and another with a force gage. According to calibration test results, a formula for transferring the oil pressure to a line load was composed. (calibration of testing apparatus is more thoroughly described in Appendixes)

After performing a laboratory test on short span sandwich panel and numerical analysis calculations, it was clear that panel is sensitive to local deflections. To avoid any local effects of load points, a low-density EPS (extruded polystyrene) block was placed under each loading beam of cylinders.

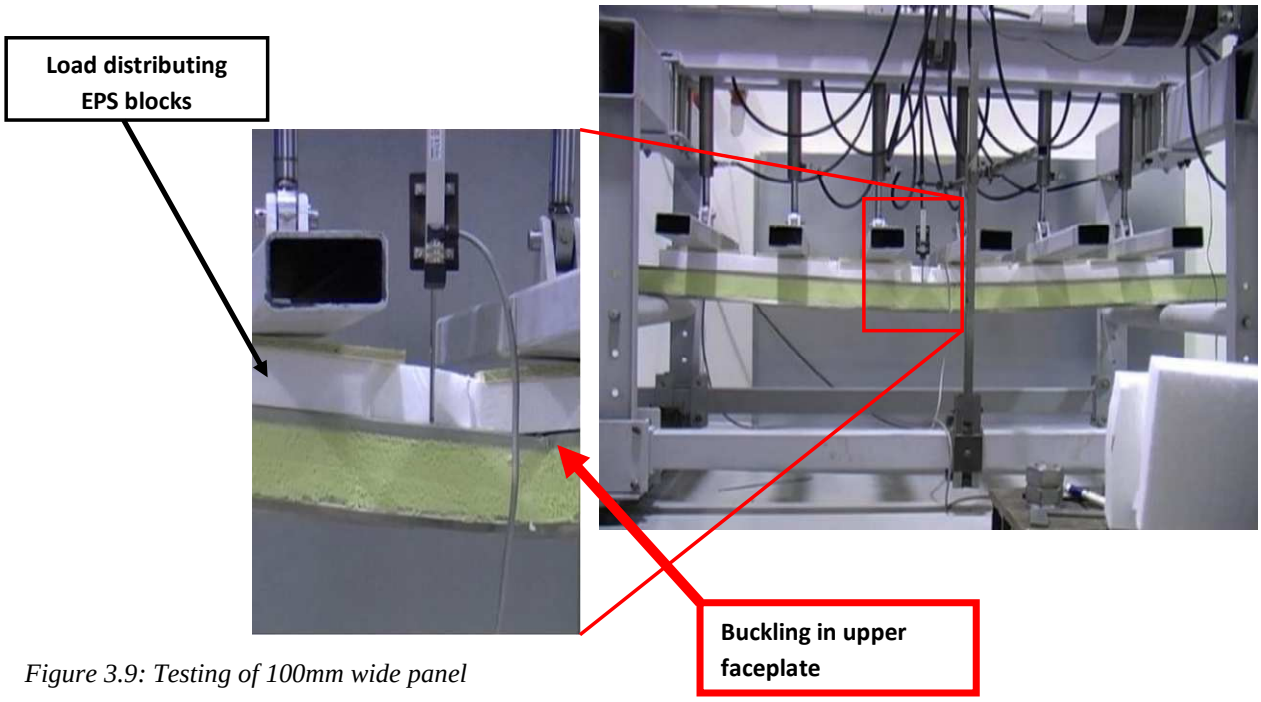

Figure 3.9: Testing of 100mm wide panel

The maximal registered carrying load was 6,68kN, which is equal to 37kPa of distributed load and the stiffness was 221N/mm.

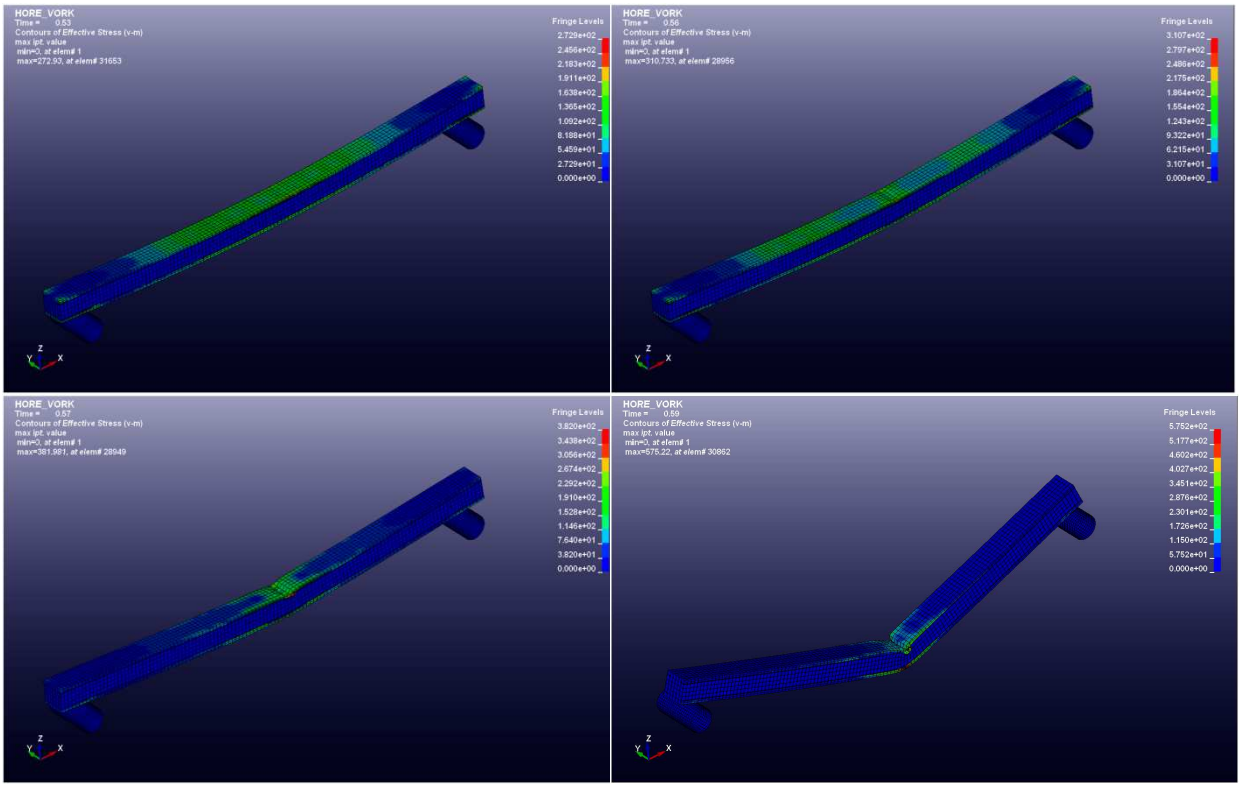

Figure 3.10: Numerical modelling of the long span beam bending (von Mises stress)

Panel failed due loss of stability in upper (compressed) plate. Stress of loosing stability (wrinkling) could not be calculated with a wrinkling equation, presented in paragraph 3.2 due large affect of the C-shape flanges on both sides of panel (see figure 2.1).

Previously defined material parameters were used in the numerical model. The panel was divided into 6 elements in thickness and in width - element edge length 16.67mm. Same element size was used on longitudinal direction. A smaller element size model was also used to ensure that chosen element size is small enough that it would not have effect on the results. The total number of elements in this model was 64960 (support-roller elements included)

Numerical modelling results were in good correlation with laboratory test results. The total carrying load in real test was 6.68 kN, which was achieved by all three specimens. In FEM calculation the total force was 5.94 kN – 11% lower compared to laboratory results. Stiffness, in terms of load-deformation, differentiated by 8% (k_{TEST} = 221 N/mm, k_{FEM} = 203 N/mm). The stiffness variation among three specimens was minimal as seen on the figure 2.5.

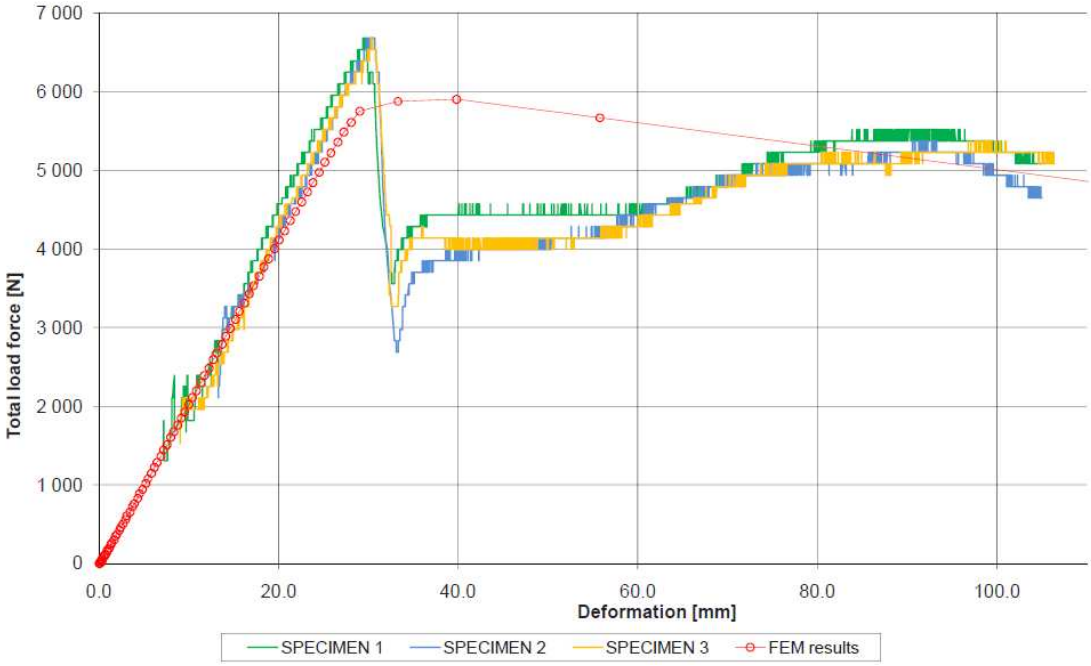

Figure 3.11: Test results of beam-like sandwich construction (1800mm span)

In terms of bending moment, the maximal carrying moment equals to:

$$M = \frac{q \cdot \ell^2}{8} = \frac{F \cdot \ell^2}{w \cdot \ell \cdot 8} = \frac{6.68 \cdot 1.8^2}{0.1 \cdot 1.8 \cdot 8} = 15.03 kNm \quad per \quad m, \qquad [3.1]$$

if to imagine that panel is used just in walls of 2.1m high cold-rooms, the maximal hydrostatic pressure that panel can stand is calculated as following.
It is assumed that the sandwich panel works as beam on two supports with a linearly decreasing line load as shown in following scheme (Figure

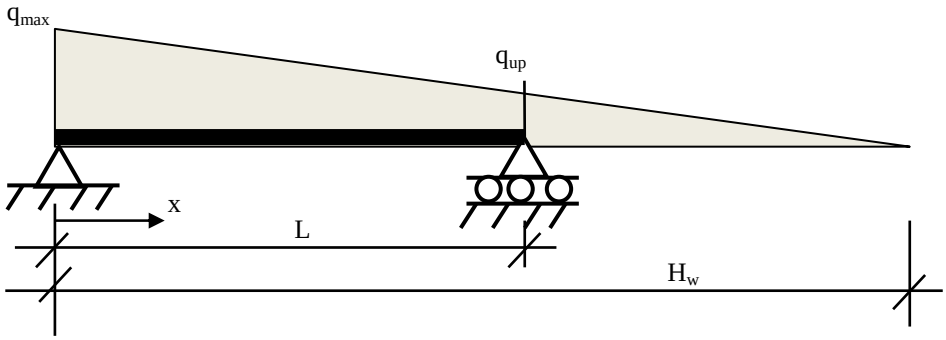

Figure 3.12 A Scheme of panel boundary conditions and loading

$L = 2030\ mm\ (lenght\ of\ a\ span)$

$H_w -\ height\ of\ water\ column\ generating\ pressure$

$q_{max} = H_w \cdot 0.00981 \quad [N/mm\ \ per\ 1m\ wide\ panel]$

$q_{up} = (H_w - L) \cdot 0.00981 \quad [N/mm\ \ per\ 1m\ wide\ panel]$

$$M(x) = \left[\left(\frac{q_{up} \cdot L}{2} + \frac{q_{max} - q_{up}}{2} \cdot L\right) \cdot x - q_{max}\left(1 - \frac{x}{H_w}\right) \cdot \frac{x^2}{2} - \left[q - \left(1 - \frac{x}{H_w}\right) \cdot q\right] \cdot \frac{x^2}{3}\right] \qquad [3.2]$$

Easiest to find needed value is just to try several H_w-s until the maximal bending moments become equal to previously found value M = 15.03 kNm. The location of maximal bending moment can easily be found if to define function for shear force and look for zero-value of the function.

$$Q(x) = L \cdot \left(\frac{q_{max} - q_{up}}{3}\right) - \frac{2x}{3}\left[q_{max} + q_{max}\left(\frac{x}{H_w} - 1\right)\right] + \frac{L \cdot q_{up}}{2} + \frac{x^2 \cdot q_{max}}{6H_w} + q_{max} \cdot x \cdot \left(\frac{x}{H_w} - 1\right) \qquad [3.3]$$

It was found that tested narrow sandwich panel stands hydrostatic pressure (H_w) 3.98 m of water column.

These results cannot be used for the estimation of collapsing load of whole panel or wall, because of the relatively high affect C-shape cold-rolled edges. These edges increase significantly the stability of compressed faceplate.

In the figure 3.11 a significant difference (laboratory tests vs. FEM results) in load carrying capacity after the loss of stability can be seen. This was caused by different loading methods – in numerical modelling, the loading force is under control, while in laboratory the displacement of the hydraulic cylinders is controlled. As the specimen fails, the oil pressure in system falls until the cylinders achieve the same displacement as the specimen has deflected.

In late stage of the test, where the carrying capacity is determined by formed plastic hinges, a quite good correlation in different tests can be seen.

3.4 Bending tests and analysis of wide sandwich panel

The test was carried out on a same bending bench that was used for bending of 100mm wide panel and the results were saved similarly. Deformation transducer was placed in the middle of the specimen in terms of longitudinal as well in perpendicular direction. Tested panel was covered with EPS sheets prior the loading to avoid local failure of upper faceplate due to contact.

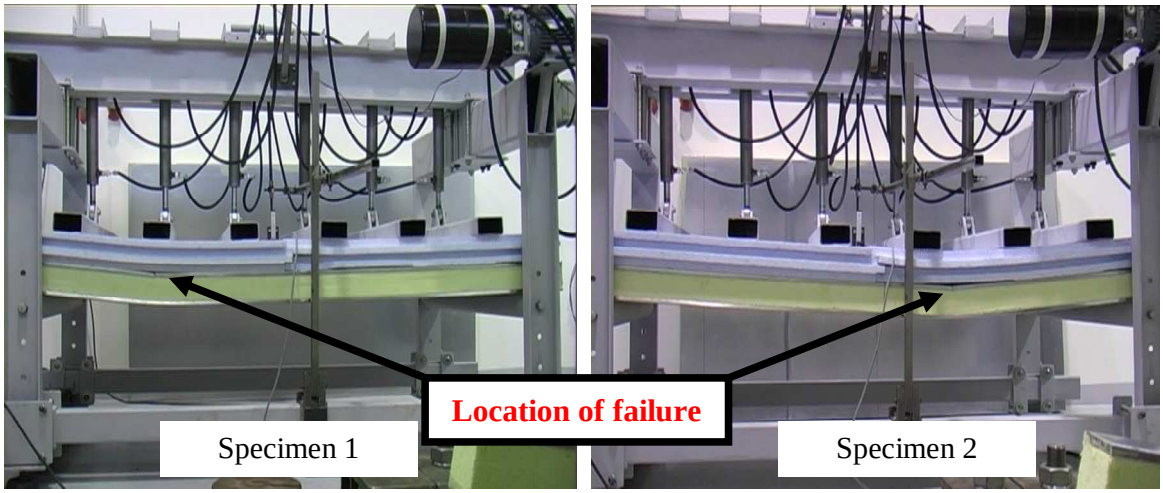

Figure 3.13 Testing of 1200mm wide sandwich panels

The panel was subject to gradually increasing distributed load until the failure, caused by loss of stability in the compressed plate. Post-buckling testing was executed until total damage of specimen to examine the plastic carrying capacity of the sandwich panel. Two
tested specimens had quite different maximum carrying load. First panel resisted 48,4kN, while second just 39,3kN – difference 19%. It must be admitted that the location of wrinkling differed also in quite large scale – first specimen lost stability just 0.26L (L – span) and second 0.37L. In both cases the distance from the middle (0.5L), where the bending moment is the largest, is rather large. The described phenomenon rather refers to defects of panel.

After the testing, a specimen was carefully cut along the wrinkling line to find any defects in face-sheets as well in core. Just by visual inspection, no defects were found. The PU-foam core seemed smooth and almost without any larger air-bubbles. Without knowing the exact technological process of the production of the panels, it is difficult to raise any other hypothesis, why the panel did not fail exactly in the middle of the span.

In numerical model, previously determined material properties were used. Panel was divided into 6 elements in height, into 72 elements in width and into 120 elements in length – 16.67x16.67x16.67mm cubes were used as elements. Face-sheets were divided into same dimensions (16.67x16.67mm) plate elements. The total number of elements in model was 79 100 (together with the support rolls).

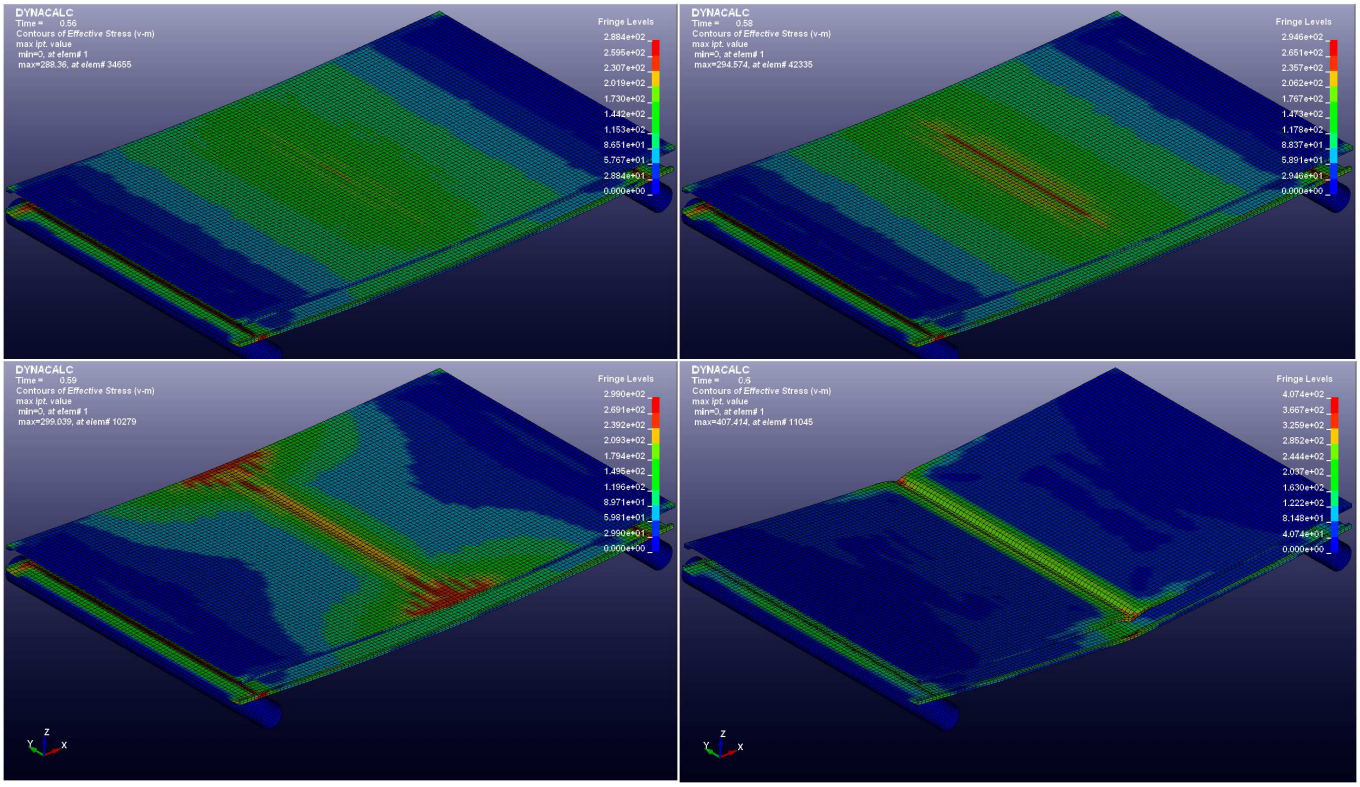

Figure 3.14 Numerical modelling of a sandwich panel (von Mises stress)

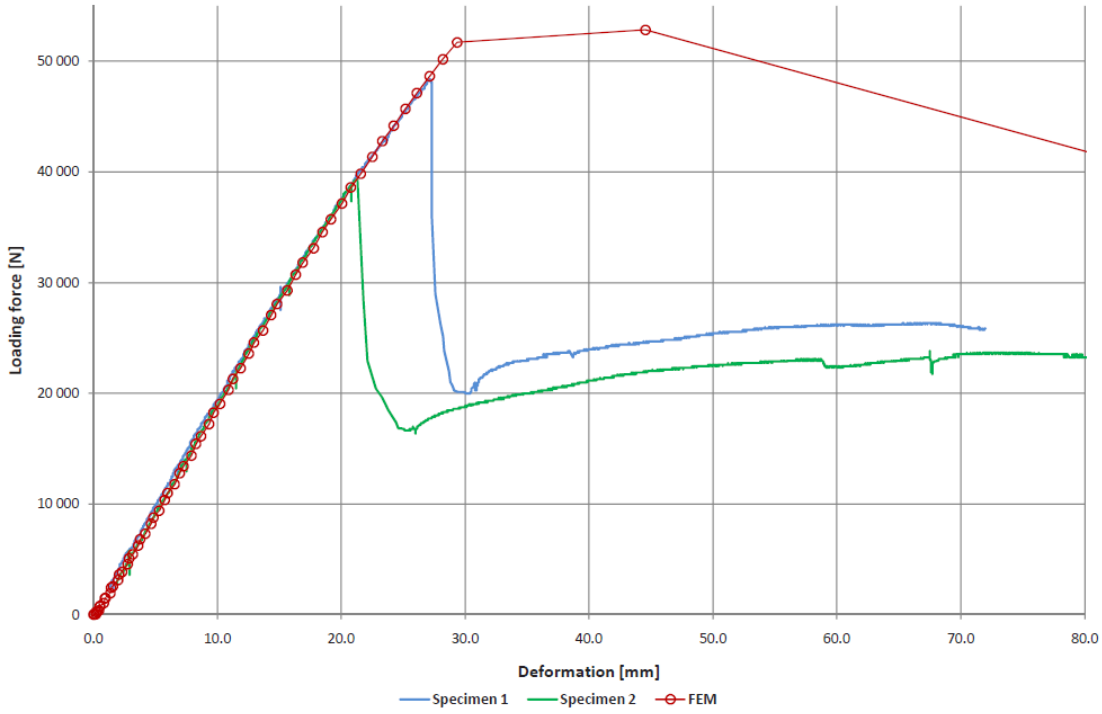

Figure 3.15 Results of 1200mm wide sandwich panel bending test

First specimen test results were in relatively good correlation to FEM results – the stiffness of panels was exactly same and the maximum carrying load differed just 6.4% (max. carrying load respectively 51.7 kN and 48.4kN). Second panel failed under 39.3 kN – 24% lower than estimated. Although it was

expected that panel in numerical model will fail under little smaller load as the failure occurred exactly in the middle of a span. Such behaviour of specimens leads to hypothesis that the core in the middle part of panel was relatively higher density compared to location where the failure occurred.

It was noticed that the ultimate strength was defined by the wrinkling of compressed plate. In all long span cases panel did fail due local buckling of upper faceplate – wrinkling of face-sheet. The longitudinal stress of upper face-sheets relatively to total loading force can be seen in figure 3.16 and similar stress value was found by analytical equation [1]:

$$\sigma_{cr} = 1.89\left[\frac{8(1-\nu_C)^2}{12(1-\nu_F^2)(1+\nu_C)(3-4\nu_C)^2}\right]^{\frac{1}{3}}(E_C G_C E_F)^{\frac{1}{3}} \qquad [3.4]$$

if E_C = 5.3 MPa (compression)
E_F = 210 000 MPa
G_C = 2.65 MPa (evaluated through Possion's ratio)
ν_C = 0.0
ν_F = 0.3

then

σ_{cr} = 117,5 MPa

Many similar formulas for calculating the wrinkling stress have been developed. Most of them having form:

$$\sigma_{wr} = K(E_C G_C E_F)^{\frac{1}{3}}, \qquad [3.5]$$

where K is a numerical constant. The value of K for design is usually around 0.65 due considerations of non-linearity of core foam, lack of flatness of faceplates, but in general varying between 0.5 and 0.95. Previous formula is bounded with any assumptions as: Poission's ratio of core is infinite and Poisson's ratio of face-sheet is 0.3. Although, no equations for estimating the wrinkling stress if the core's Young's modulus differs in tension and compression have been developed yet.

Nevertheless, maximum bending moment of panel can be calculated according to previously found critical wrinkling stress:

$$M_{analytical} = \sigma_{cr} \cdot h \cdot t = 110{,}2 \cdot 100 \cdot 0.6 = 7050 Nmm/mm \qquad [3.6]$$

According to maximum carrying load from FEM results, the distributed load per longitudinal unit is 28.7 N/mm. Moreover, the maximum bending moment can be calculated:

$$M_{FEM} = \frac{q \cdot L^2}{8 \cdot b} = \frac{28.7 \cdot 1800^2}{8 \cdot 1200} = 9686 Nmm/mm \quad [3.7]$$

Third possible way to determine the maximal carrying momentum of bending is according the real test results, similarly to FEM calculation results. Distributed load calculated according maximal carrying load is calculated: 48400/1800 = 26.89 N/mm

$$M_{lab\_test} = \frac{q \cdot L^2}{8 \cdot b} = \frac{26.9 \cdot 1800^2}{8 \cdot 1200} = 9079 Nmm/mm \quad [3.8]$$

These calculations give a hint that C-shape flanges increase the stability of faceplate as well the ultimate strength of the panel significantly.

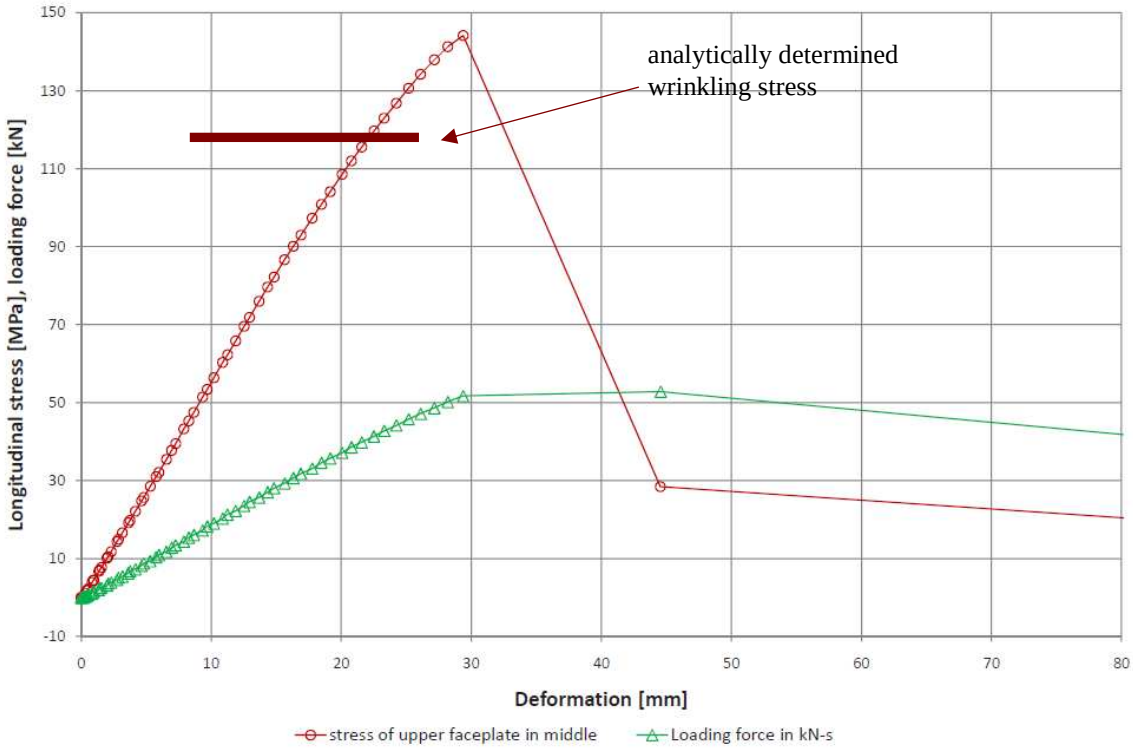

Figure 3.16 Comparison of stresses in the middle of upper faceplate and total loading force

3.5 Testing of cold-room panel connections

The aim of the testing was to examine the strength and the stiffness of panel connections for determining the connections properties and finding parameters of boundary conditions in numerical calculations. In general, two types of testing were carried out – bending (cantilever) and shear testing.

3.5.1 Connections share-testing

In shear testing, only the total carrying force for was under investigation as the deformations were relatively small and differed in large scale from specimen to other. On the other hand, maximum carrying capacities among specimens were in general the same as seen also in figure 3.17. The maximum shear carrying capacities were 16 196 N and 16051 N.

For better visualisation, in the figure 3.17, the deformation on horizontal axes is replaced with timeline of the test, as the loading rate among specimens was almost the same.

Found maximal carrying values of connections were used in the design of numerical model, as the modelling of all small details of the connection locks would have been time-consuming and inefficient in terms of reliability in results.

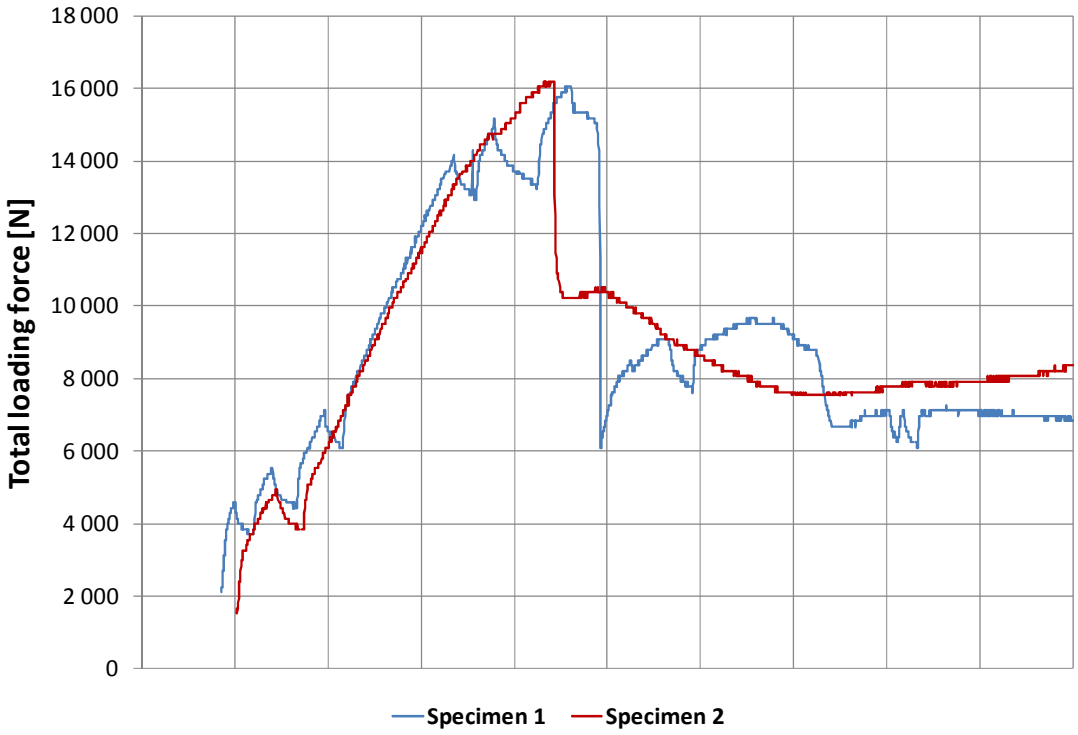

Figure 3.17 Laboratory share testing on straight connections

3.5.2 Connections bend-testing

The main aim of bending test of the straight panel connection was to find the stiffness difference between connection and panel without connections. Such information helps to determine stiffness of the connection elements in model as well as to define the boundary conditions for whole wall.

In the figure 3.18 can be seen that the corner connection had slightly larger stiffness, but after the failure the carrying capacity fell quite rapidly. The straight connection, on the other hand, had smaller stiffness, but did not have any clear point of failure and could stand relatively high loading also during large deformations.

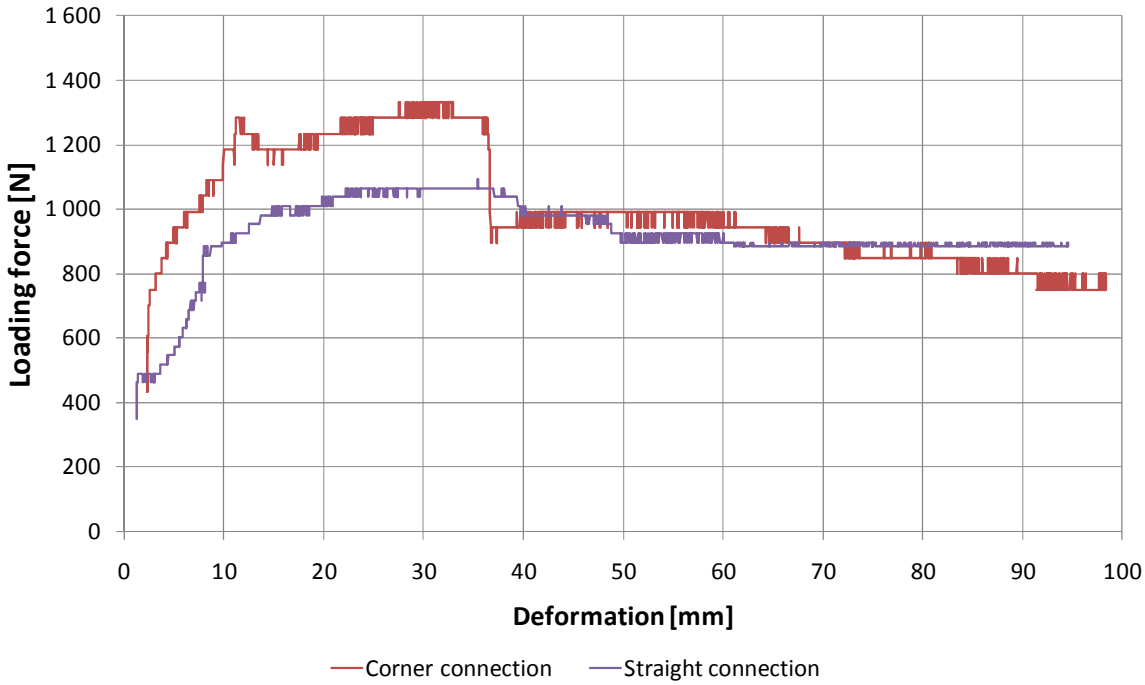

Figure 3.18 Laboratory bending testing of corner and straight connection

The comparison of cross-section moments in continues panel and in straight panel connection

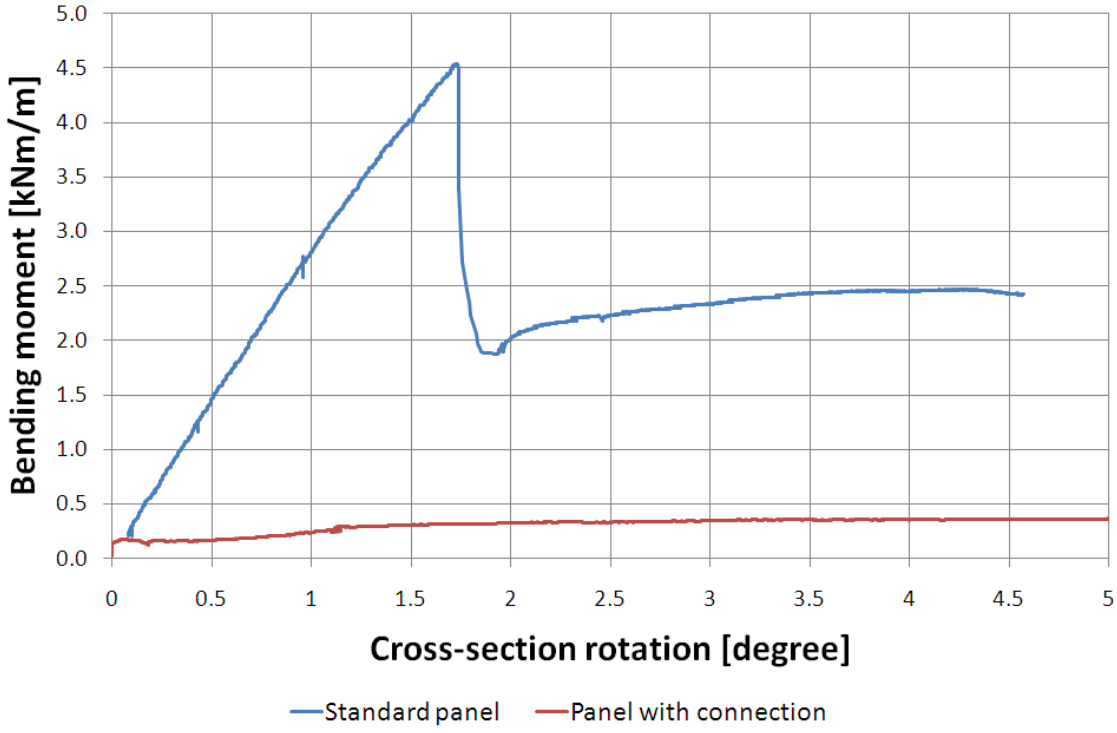

Figure 3.19 Comparison of panel with and without a connection

seen in figure 3.19. If to be interested just in stiffness of elastic phase of testing then the calculated stiffness difference is 93 times in terms of ascent ratio of graphs. In terms of difference in bending moment at 1.68 degrees, the difference is 14.2 times.

The lock of the panel is also designed to carry just the shear force not the bending moment, as the connecting element is exactly in the centre of a panel (in thickness).

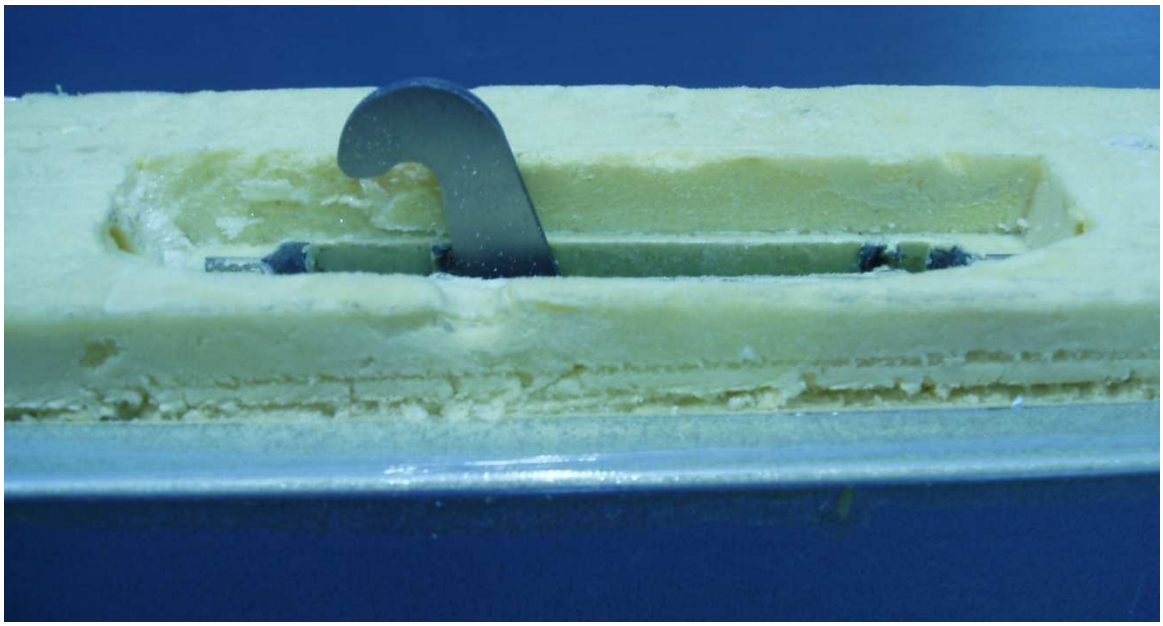

Figure 3.20 Connecting element in sandwich panel locks

As conclusion, it must be said that the bending stiffness of connections is very low compared to original panel and in numerical model the connections can be designed just to carry the shear stresses without any bending stiffness. These test results also gave the reason to design the wall edges as simply supported panel for analytical solution.

4. COLLAPSE STRENGHT OF COLD-ROOM WALL UNDER HYDROSTATIC PRESSURE

4.1 Numerical simulation of cold-room wall under hydrostatic pressure

Modelling element size was kept the same as in single panel modelling. Boundary conditions were described as similar to real conditions as possible – connecting elements in the middle of the thickness of panel (for more details, see paragraph 3.5). Continuous welding on inner side of the wall was replaced in the model with very frequent spot-welds that the strengths real case and in model were equal. Outer side was freely supported by a L-profile. Wall shorter sides were freely supported by the same type walls that represent perpendicular walls in real case. Again, the locking equivalent elements were designed at corner connections.

Load was applied from inside gradually increasing, (according to cosine function from 180 degrees to 270) in two parts – triangular (represents hydrostatic pressure up to upper edge of wall) and rectangular (represents hydrostatic pressure over the upper edge of wall) distributed loading. A triangularly distributed load reached its maximum value in one third of the calculation time and after that, the gradually increasing rectangular load was applied. Loading scheme is shown in the following figure (figure 4.1).

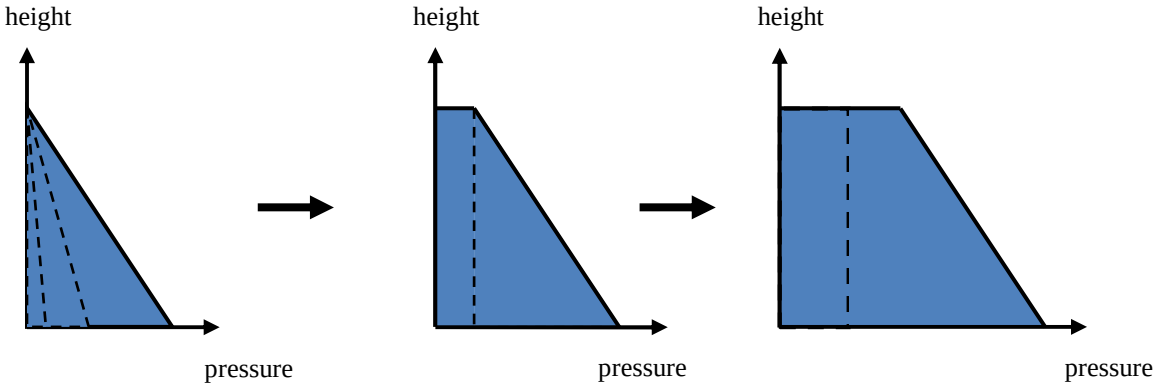

Figure 4.1 Scheme of loading

Similar to an envelope type plastic hinge failure mode was noticed while registered carrying capacity was 2.75 m hydrostatic pressure for 5m long wall and 2.57 for 8m long wall. Actually, before the plastic hinge from the corners formed, a horizontal line was already established. That failure behaviour and loading values were noticed with first model of sandwich cold-room. The first model of sandwich wall was constructed before the tests on connections were performed. Thus, the first model was made of single panel as seen in figures 4.3 and 4.4. In that model shorter edges of the wall were simply supported.

After the connections testing, a new model with individual panels and connecting elements between them was constructed. In this model the shorter edges were also simply supported, but also connected to supporting wall with connection elements.

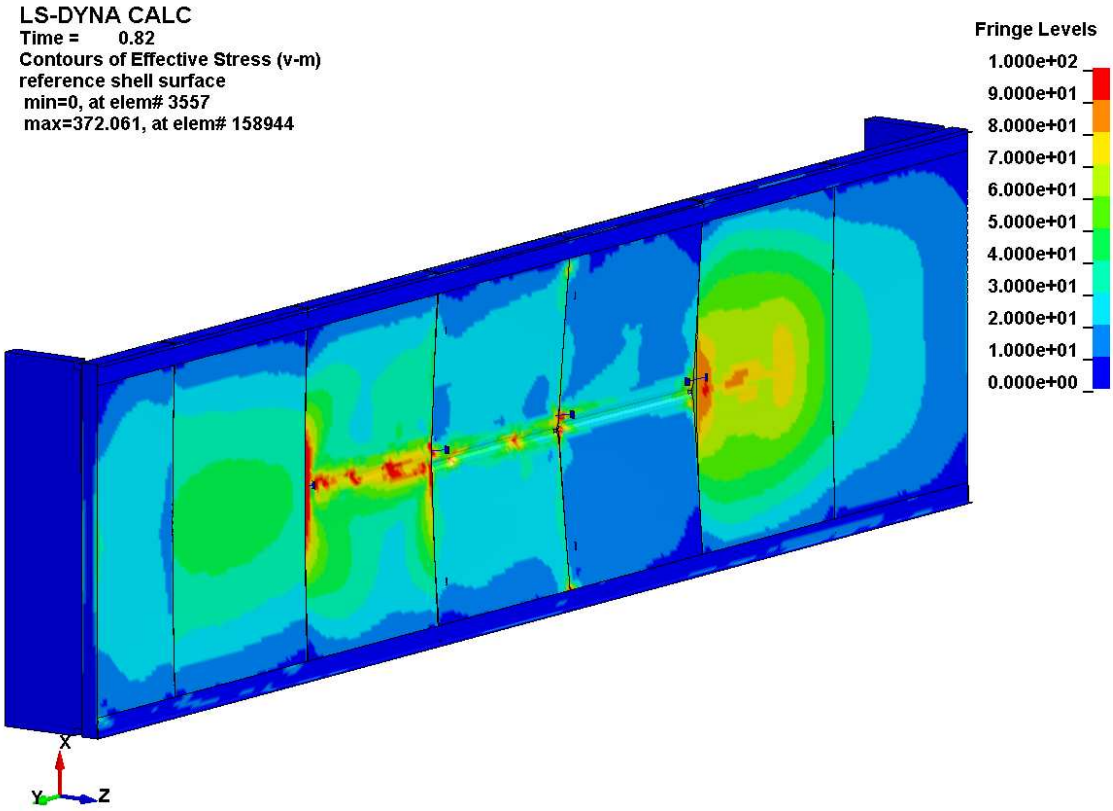

Figure 4.2 8m-long cold-room wall failure

Load carrying capacity of individual panels wall was exactly the same as single panel wall. This phenomenon supports the idea described in paragraph 4.2 that the ultimate strength is mainly determined by the shorter span of panels/wall. The deflection of the wall, on the other hand, differed in very large scale if to compare the first model and the second. That seems normal, as the stiffness along connection lines is almost zero, as described in paragraph 3.5.2. Failure of individual panels wall can be seen in figure 4.2.

4.2 Analytical methods for collapse estimation of cold-room wall

Reasoned by the envelope failure type an analytical solution for freely supported plate was generated. It was presumed that the work done by the load is equal to work, done by the plastic hinges. This analytical solution was because such plastic hinge lines could be easily seen on previous FEM analyses.

To compare different analytical approaches for sandwich structure, a horizontal line plastic hinge was under examination. Such model describes very well the failure if the wall would be much wider compared to the height. For example, it would be accurate model for infinitely long wall.

Two previously mentioned plastic hinge methods gave reasonably accurate results in certain cases (specific wall height and width), but in some cases gave quite poor results. Conditioned by uncertainty

of models, elastic state energy balance model for a plate was applied to estimate cold-room structure strength. The Navier approach of rectangular plate was used for solving the model.

4.2.1 Model, based on envelope shape failure mode

Plastic hinge based load carrying capacity was determined by the wrinkling stress in the compressed plate. Internal work was found by adding all the work done by plastic hinges.

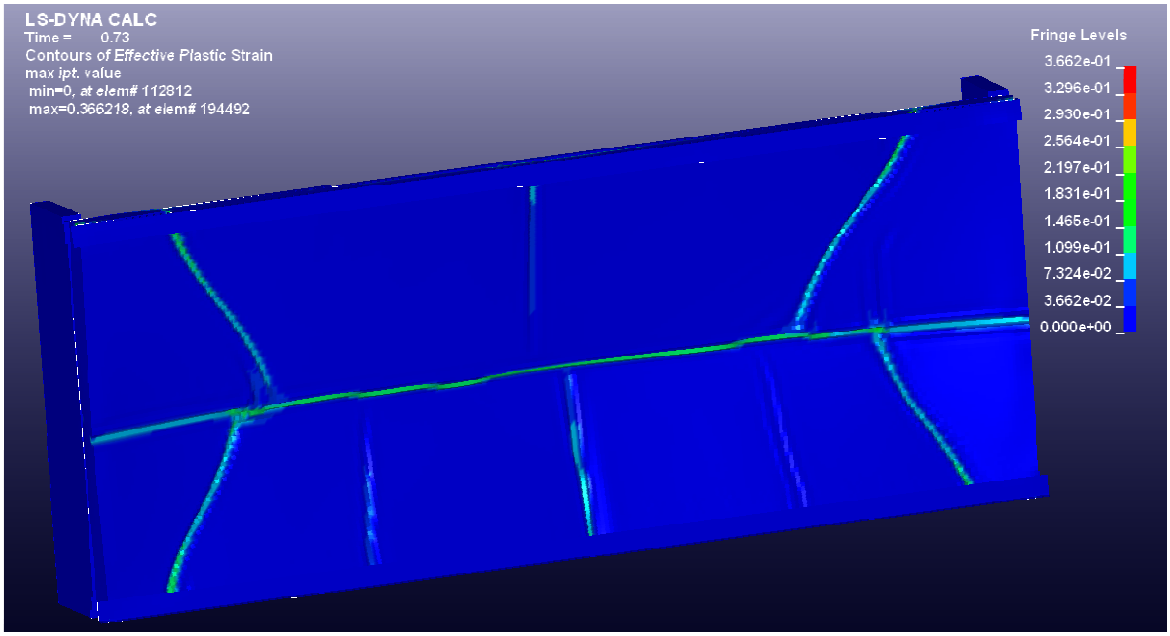

Figure 4.3 Numerical modelling of a cold room wall (plastic strain)

Finding the external work, the rotated planes were described mathematically to create the formed surface and the distributed load was integrated over the this surface. The ultimate carrying capacities estimated by the analytical solution were significantly larger compared to FEM results. Exact carrying capacities were 3.64m (+32.4% compared to FEM values) and 3.25m (+26.5%) respectively to 5m and 8m long walls.

4.2.2 Model, based on single yield line failure mode

Analysing the deformation of wall in the numerical modelling it can be seen that before the plastic hinges from the corners are formed the horizontal plastic hinge has reached from side to side. According to this phenomenon and too high carrying capacity of envelope shape plastic hinge, an analytical solution for single horizontal plastic hinge type failure was created.

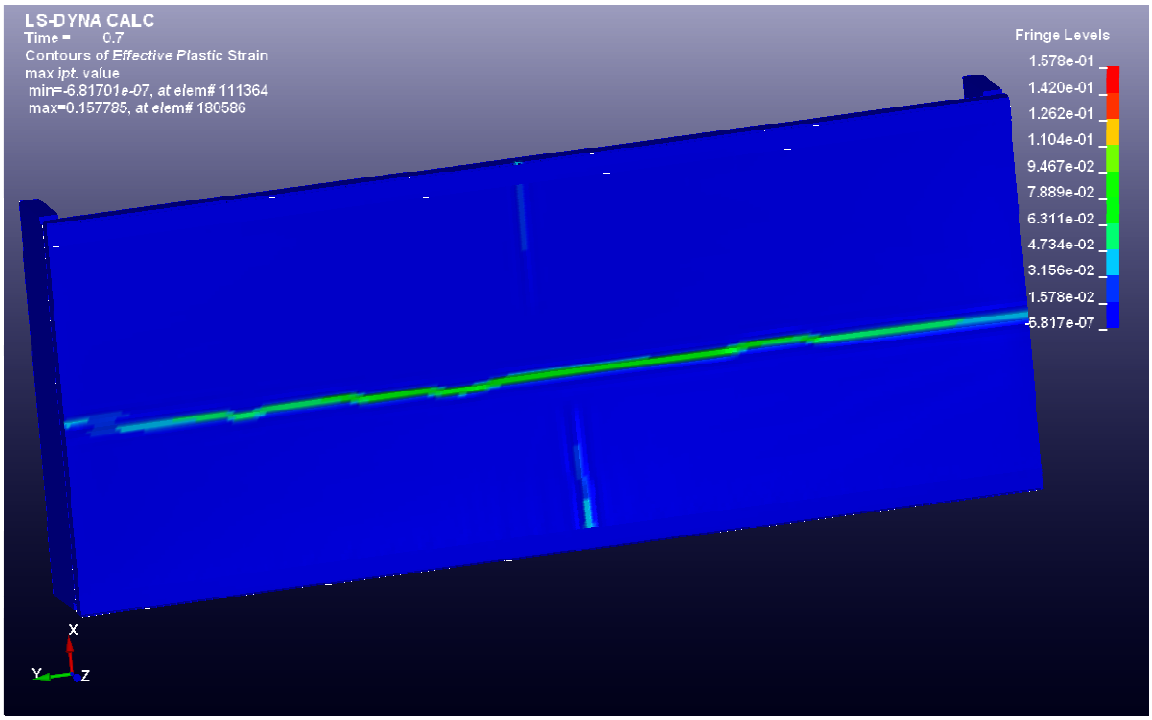

Figure 4.4 Numerical modelling of a cold room wall (plastic strain)

Presumptions of the analysis were same as in previous solution. The ultimate load carrying capacities were closer to FEM results (3.12m (+13.3%) for 5m long wall and 3.12m (+21.4%) for 8m long wall), but as this solution is not wall-length-dependent, it cannot be considered as adequate equation for estimating the ultimate hydrostatic carrying capacity.

4.2.3 Model, based on elastic plate bending

According to plate theory and the Navier approach of rectangular plate an analytical solution about elastic behavior of plate was created.
This solution can be used, as the stiffness supporting corners is almost zero. Another criteria of the use of model is that must be met is that the deformations should be relatively small – plate in elastic state.

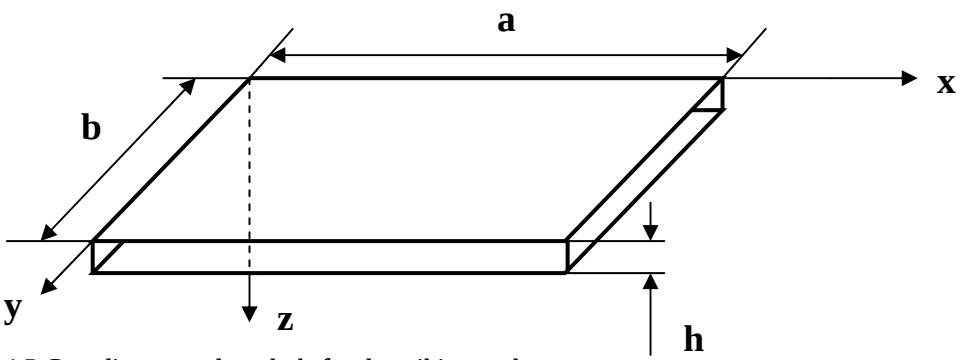

Figure 4.5 Coordinates and symbols for describing a plate

Derivation for elastic plate using Navier's solution:

$$\frac{\partial^4 w}{\partial x^4} + 2\frac{\partial^4 w}{\partial x^2 \partial y^2} + \frac{\partial^4 w}{\partial y^4} = \frac{p(x,y)}{D}$$ (classical plate equation)

Free supported plate surface can be described by double trigonometric series. The choice of the trigonometric functions used for the deflection is restricted to those that satisfy the boundary conditions of the problem. Simply supported boundary conditions are:

$$w_0(0,y) = 0, \quad w_0(a,y) = 0, \quad w_0(x,0) = 0, \quad w_0(x,b) = 0, \quad M_{xx}(0,y) = 0,$$

$$M_{xx}(a,y) = 0, \quad M_{yy}(x,0) = 0 \text{ and } M_{yy}(x,b) = 0$$

and are met by the following form of the transverse deflection:

$$w(x,y) = \sum_{m=1}^{\infty}\sum_{n=1}^{\infty} C_{mn} \sin\frac{m\cdot\pi\cdot x}{a}\sin\frac{n\cdot\pi\cdot y}{b}$$

The loading must be also presented in similar formula and thus it has to be expanded into Fourier series:

$$p(x,y) = \sum_{m=1}^{\infty}\sum_{n=1}^{\infty} B_{mn} \sin\frac{m\cdot\pi\cdot x}{a}\sin\frac{n\cdot\pi\cdot y}{b}$$

The factors B_{mn} will be found by using following formulas:

$$B_{mn} = \frac{4}{ab}\int_0^a\int_0^b p(x,y)\sin\frac{m\cdot\pi\cdot x}{a}\sin\frac{n\cdot\pi\cdot y}{b}dxdy$$

As next step, the equations of *w* (deformations) and *p* (loading) must be substituted into elastic plate equation:

$$\sum_{m=1}^{\infty}\sum_{n=1}^{\infty} C_{mn}\left[\left(\frac{m\cdot\pi}{a}\right)^4 + 2\cdot\left(\frac{m\cdot\pi}{a}\right)^2\left(\frac{n\cdot\pi}{b}\right)^2 + \left(\frac{n\cdot\pi}{b}\right)^4\right]\sin\frac{m\cdot\pi\cdot x}{a}\sin\frac{n\cdot\pi\cdot y}{b} = \frac{1}{D}\sum_{m=1}^{\infty}\sum_{n=1}^{\infty} B_{mn}\sin\frac{m\cdot\pi\cdot x}{a}\sin\frac{n\cdot\pi\cdot y}{b}$$

As previous equation must be apply with every m and n, then:

$$C_{mn} = \frac{B_{mn}}{\pi^4\cdot D\left[\left(\frac{m}{a}\right)^2 + \left(\frac{n}{b}\right)^2\right]^2}$$

$$w(x,y) = \frac{1}{\pi^4\cdot D}\sum_{m=1}^{\infty}\sum_{n=1}^{\infty}\frac{B_{mn}}{\left[\left(\frac{m}{a}\right)^2 + \left(\frac{n}{b}\right)^2\right]^2}\cdot\sin\frac{m\cdot\pi\cdot x}{a}\sin\frac{n\cdot\pi\cdot y}{b}$$

In our case:

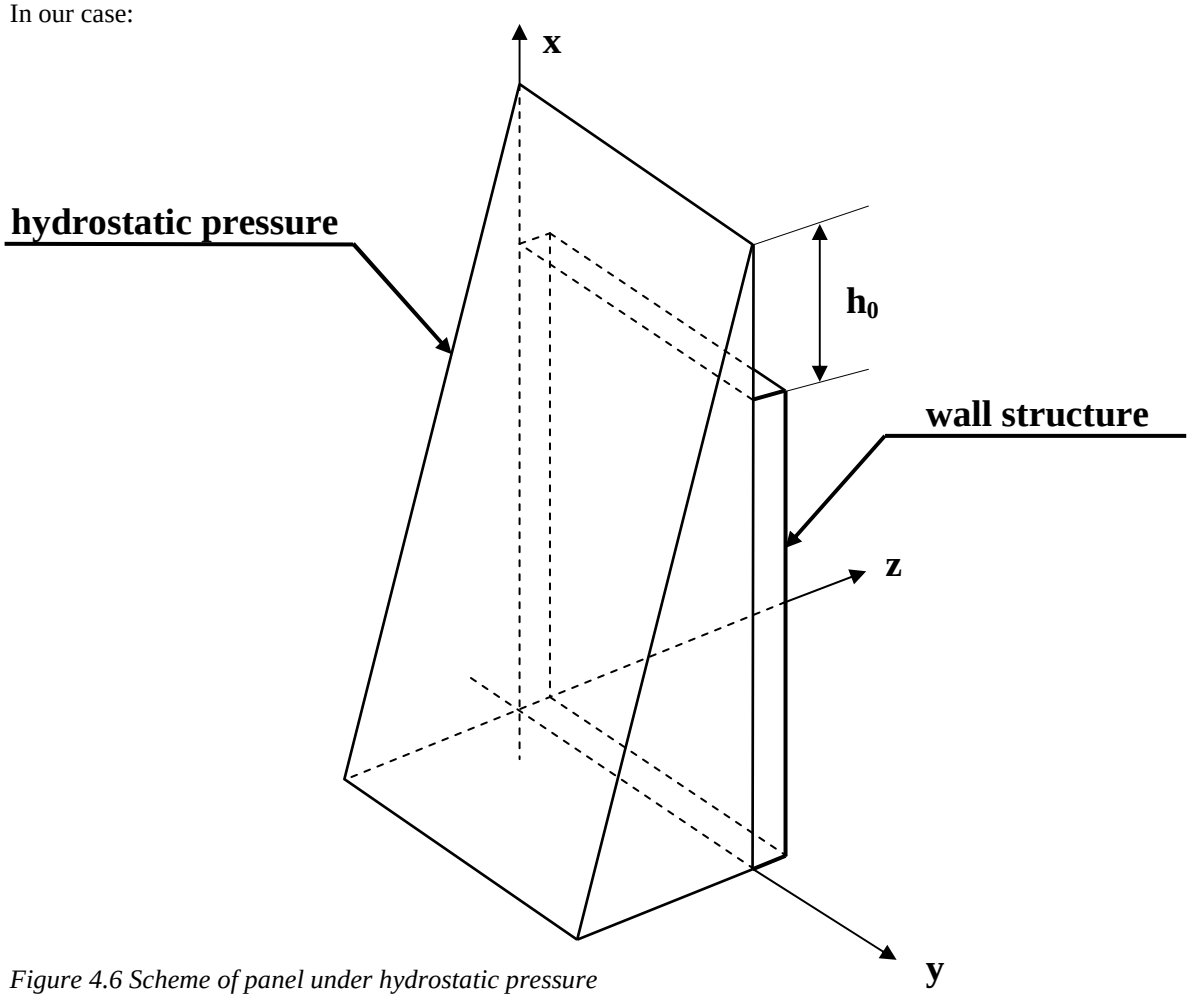

Figure 4.6 Scheme of panel under hydrostatic pressure

The loading is defined:

$$p(x, y, h_0) = \rho \cdot g \cdot x + \rho \cdot g \cdot h_0$$ where:

ρ – density of water

g – gravity acceleration

h_0 – height of water column over the top end of wall structure

x – distance from bottom end of wall

For finding constants B_{mn}, the loading equation was divided and integrated separately:

$$B_{Amn} = \frac{4}{ab}\int_0^a\int_0^b \rho \cdot g \cdot x \sin\frac{m\cdot\pi\cdot x}{a}\sin\frac{n\cdot\pi\cdot y}{b}dxdy = \frac{8a\cdot g\cdot\rho}{\pi^3\cdot m^2\cdot n}\cdot\sin\left(\frac{\pi\cdot n}{2}\right)^2\cdot\left[\sin(\pi\cdot m)-\pi\cdot m\cdot\cos(\pi\cdot m)\right]$$

$$B_{Bmn} = \frac{4}{ab}\int_0^a\int_0^b \rho \cdot g \cdot \sin\frac{m\cdot\pi\cdot x}{a}\sin\frac{n\cdot\pi\cdot y}{b}dxdy = \frac{16\cdot g\cdot\rho}{\pi^2\cdot m\cdot n}\cdot\sin\left(\frac{\pi\cdot m}{2}\right)^2\sin\left(\frac{\pi\cdot n}{2}\right)^2$$

$$p_A = \frac{8a\cdot g\cdot\rho}{\pi^3\cdot m^2\cdot n}\cdot\sin\left(\frac{\pi\cdot n}{2}\right)^2\cdot\left[\sin(\pi\cdot m)-\pi\cdot m\cdot\cos(\pi\cdot m)\right]$$

$$p_B = \frac{16 \cdot g \cdot \rho}{\pi^2 \cdot m \cdot n} \cdot \sin\left(\frac{\pi \cdot m}{2}\right)^2 \sin\left(\frac{\pi \cdot n}{2}\right)^2$$

Now can constants B_{mn} written in form:

$$B_{mn} = p_A + p_B \cdot h_0 = \left[\frac{8 \cdot g \cdot \rho}{\pi^2 \cdot m \cdot n} \cdot \sin\left(\frac{n \cdot \pi}{2}\right)^2\right] \cdot \left[\left[\frac{a}{\pi \cdot m} \cdot \left(\sin(\pi \cdot m) - \pi \cdot m \cdot \cos(\pi \cdot m)\right)\right] + \left(2 \cdot h_0 \cdot \sin\left(\frac{\pi \cdot m}{2}\right)^2\right)\right]$$

$$p(x, y, h_0) = \sum_{m=1}^{k} \sum_{n=1}^{k} \left[\left(p_A + p_B \cdot h_0\right) \cdot \sin\left(\frac{m \cdot \pi \cdot x}{a}\right) \cdot \sin\left(\frac{n \cdot \pi \cdot y}{b}\right)\right],$$

hence the transverse deflection can be written:

$$w(x, y, h_0) = \frac{1}{\pi^4 \cdot D} \sum_{m=1}^{\infty} \sum_{n=1}^{\infty} \frac{\left[\left(p_A + p_B \cdot h_0\right)\right]}{\left[\left(\frac{m}{a}\right)^2 + \left(\frac{n}{b}\right)^2\right]^2} \cdot \sin\frac{m \cdot \pi \cdot x}{a} \sin\frac{n \cdot \pi \cdot y}{b}$$

$$w(x, y, h_0) = \frac{1}{\pi^4 \cdot D} \sum_{m=1}^{\infty} \sum_{n=1}^{\infty} \frac{\left[\frac{8 \cdot g \cdot \rho}{\pi^2 \cdot m \cdot n} \cdot \sin\left(\frac{n \cdot \pi}{2}\right)^2\right] \cdot \left[\left[\frac{a}{\pi \cdot m} \cdot \left(\sin(\pi \cdot m) - \pi \cdot m \cdot \cos(\pi \cdot m)\right)\right] + \left(2 \cdot h_0 \cdot \sin\left(\frac{\pi \cdot m}{2}\right)^2\right)\right]}{\left[\left(\frac{m}{a}\right)^2 + \left(\frac{n}{b}\right)^2\right]^2} \cdot \sin\frac{m \cdot \pi \cdot x}{a} \sin\frac{n \cdot \pi \cdot y}{b}$$

It is known that for a plate the bending moment along x-axis can be expressed as:

$$M_x = \int_{-\frac{h}{2}}^{\frac{h}{2}} z \sigma_x dx = -D\left(\frac{\partial^2}{\partial x^2} w + \nu \frac{\partial^2}{\partial y^2} w\right)$$

After derivations of transverse deflection equation, the bending moment is:

$$M_x = \sum_{m=1}^{\infty} \sum_{n=1}^{\infty} \frac{\left[\left(p_A + p_B \cdot h_0\right)\right]}{\pi^2 \cdot \left[\left(\frac{m}{a}\right)^2 + \left(\frac{n}{b}\right)^2\right]^2} \cdot \left[\left(\frac{m}{a}\right)^2 + \nu_F \left(\frac{n}{b}\right)^2\right] \cdot \sin\left(\frac{m \cdot \pi \cdot x}{a}\right) \sin\left(\frac{n \cdot \pi \cdot y}{b}\right)$$

For simplified solution, it can be assumed that the maximal bending moment occurs at the half of the height. The water height over the upper edge of structure can be shown:

$$h_0 = \frac{M_p - \sum_{m=1}^{\infty} \sum_{n=1}^{\infty} \frac{p_A}{\pi^2 \cdot \left[\left(\frac{m}{a}\right)^2 + \left(\frac{n}{b}\right)^2\right]^2} \cdot \left[\left(\frac{m}{a}\right)^2 + \nu_F \left(\frac{n}{b}\right)^2\right] \cdot \sin\frac{m \cdot \pi \cdot x}{a} \sin\frac{n \cdot \pi \cdot y}{b}}{\sum_{m=1}^{\infty} \sum_{n=1}^{\infty} \frac{p_B}{\pi^2 \cdot \left[\left(\frac{m}{a}\right)^2 + \left(\frac{n}{b}\right)^2\right]^2} \cdot \left[\left(\frac{m}{a}\right)^2 + \nu_F \left(\frac{n}{b}\right)^2\right] \cdot \sin\frac{m \cdot \pi \cdot x}{a} \sin\frac{n \cdot \pi \cdot y}{b}}$$

In case for more accurate result, first the location of maximal momentum must be found. It is well known that the function achieves its maximal value in point were the first derivative is equal to zero. As first step a first derivative of momentum must be evaluated:

$$y = \frac{b}{2}$$

$$q_x(x, h_0) = \sum_{m=1}^{\infty}\sum_{n=1}^{\infty} \frac{[(p_A + p_B \cdot h_0)]}{\pi^4 \cdot \left[\left(\frac{m}{a}\right)^2 + \left(\frac{n}{b}\right)^2\right]^2} \cdot \left[\left(\frac{m \cdot \pi}{a}\right)^2 + \nu_F \left(\frac{n \cdot \pi}{b}\right)^2\right] \cdot \frac{m \cdot \pi}{a} \cdot \cos\left(\frac{m \cdot \pi \cdot x}{a}\right) \sin\left(\frac{n \cdot \pi}{2}\right) \quad [4.1]$$

The argument of this function at value zero will be found and given to x_{max}.

As next step, it is assumed that the maximum value of bending moment that wall can stand is equal to previously calculated wrinkling momentum M_p.

Hence, to find h_0 the root of derivate bending momentum formula minus plastic momentum [$q_x(x, h_0)$ - M_p] is found while $x = x_{max}$.

Root about h_0 of following function must evaluate to find more accurate h_0:

$$q_x(x = x_{max}, h_0) = \sum_{m=1}^{\infty}\sum_{n=1}^{\infty} \frac{[(p_A + p_B \cdot h_0)]}{\pi^4 \cdot \left[\left(\frac{m}{a}\right)^2 + \left(\frac{n}{b}\right)^2\right]^2} \cdot \left[\left(\frac{m \cdot \pi}{a}\right)^2 + \nu_F \left(\frac{n \cdot \pi}{b}\right)^2\right] \cdot \frac{m \cdot \pi}{a} \cdot \cos\left(\frac{m \cdot \pi \cdot x}{a}\right) \sin\left(\frac{n \cdot \pi}{2}\right)$$

If even more accurate h_0 is needed, the found h_0 must be inserted to equation and same procedure follows until required accuracy is achieved.

In current case new evaluation of h_0 is not needed as the value differed less than 1mm.

5. COLLAPSE STRENGTH OF A-60 DOUBLE LEAF HINGED DOOR

The strength estimation of A-60 double leaf hinged marine door was simpler compared to sandwich panel investigation. Material parameters were determined on producer provided technical properties of materials and on appropriate literature. First model was made of single material – ordinary structural mild steel to investigate the affect of material properties. In this model, it was observed that there are three main elements, which material strength affects the results in large scale – hinge pins, latch and latch rod of passive door leaf. Use of mild steel generated abnormally large deformations in named details, which caused the opening of the doors in quite early stage of the loading process.
Model geometry was determined by a drawing: *SA-24076 double with U-frame (3-15980 B).dwg* (19.12.2010)
In the next model, following material parameters were used:

Hinged fire-door materials

No.	Material	Material type	ρ [t/mm^3]	E [MPa]	ν	σ_y [MPa]	Tangent E [MPa]	plastic strain failure
1	**Steel**	PIECEWISE LINEAR PLASTICITY	7.85E-09	210000	0.3	250	0	0

No.	Material	Material type	ρ [t/mm^3]	E [MPa]	Tension cut-off stress
2	**Mineral wool**	LOW DENSITY FOAM	1.00E-10	10	0.1

No.	Material	Material type	ρ [t/mm^3]	E [MPa]	ν	σ_y [MPa]	Tangent E [MPa]	plastic strain failure
3	**Stainless steel**	PIECEWISE LINEAR PLASTICITY	7.85E-09	210000	0.3	250	0	0

No.	Material	Material type	ρ [t/mm^3]	E [MPa]	ν	σ_y [MPa]	Tangent E [MPa]	plastic strain failure
4	**Hinges**	PIECEWISE LINEAR PLASTICITY	7.85E-09	205000	0.29	325	200	0.18

No.	Material	Material type	ρ [t/mm^3]	E [MPa]	ν	σ_y [MPa]	Tangent E [MPa]	plastic strain failure
5	**Locking rod**	PIECEWISE LINEAR PLASTICITY	7.85E-09	210000	0.29	800	200	0.2

No.	Material	Material type	ρ [t/mm^3]	E [MPa]	ν	σ_y [MPa]	Tangent E [MPa]	plastic strain failure
6	**Lock latch, lock bolt**	PIECEWISE LINEAR PLASTICITY	7.85E-09	170000	0.3	200	200	0.07

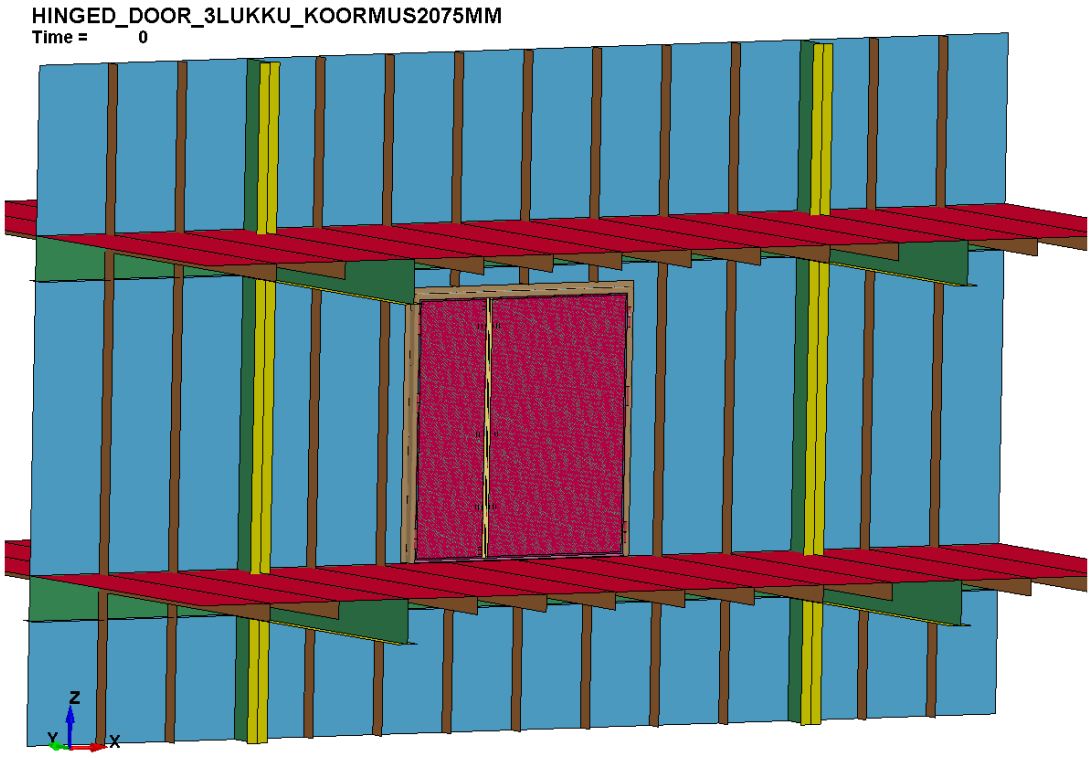

Figure 5.1 Initial position and boundary conditions of hinged fire-door

Hinged fire-door resisted load of 2.06 m (20.2kPa) of hydrostatic pressure. At this pressure active (wider) door leaf got deformations that the lock-latches came out of the strike plate pocket.

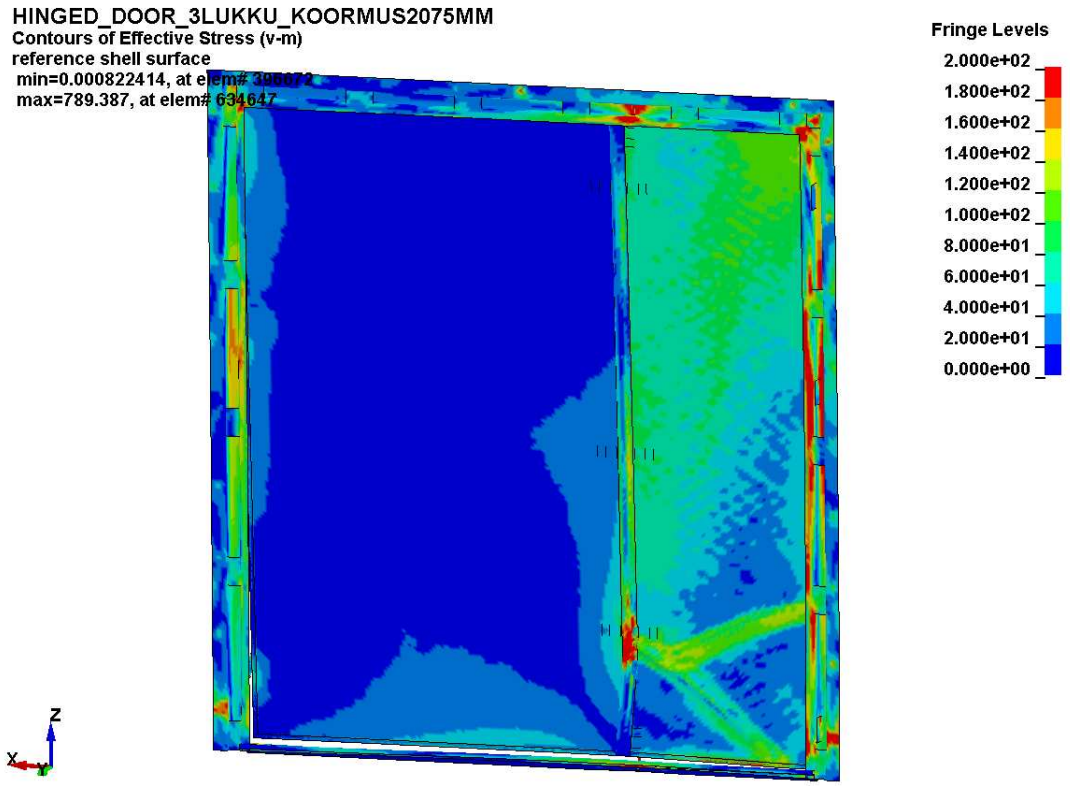

Figure 5.2 Inside of hinged fire-door at failure (von Mises stress)

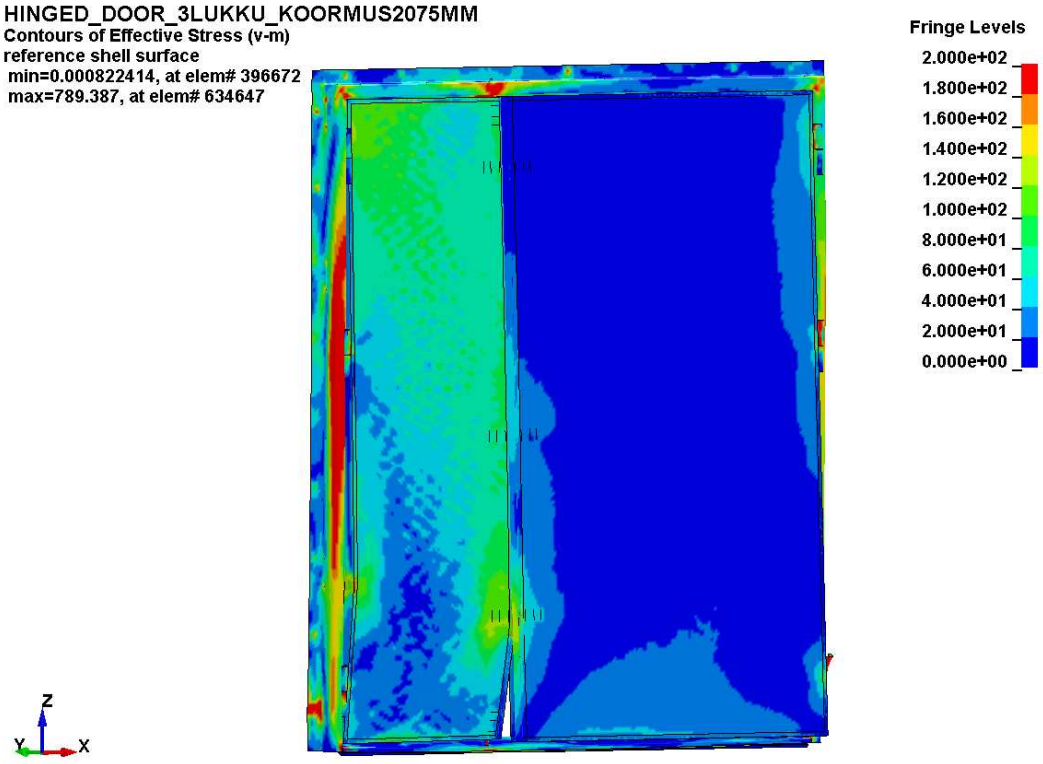

Figure 5.3 Outside of hinged fire-door at failure (von Mises equivalent stress)

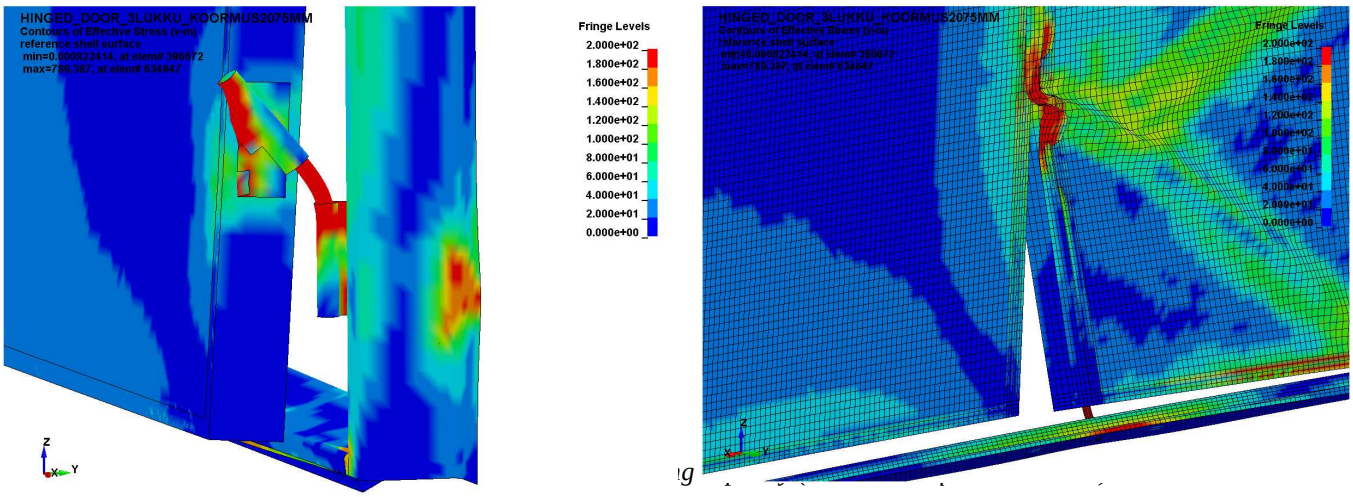

In real flooding case it might be quite rear to obtain hydrostatic difference more than 2.06 meters as the structure is not watertight.

6. COLLAPSE STRENGTH OF SWT-DOOR

The strength estimation of semi-watertight A-60 sliding door was done similarly to A-60 double leaf door. Material parameters were determined according to producer provided information.
Model geometry was determined by a drawing: *LA60WeO_a_L1363_SWT.dwg* (19.12.2010)

Sliding SWT door materials

No.	Material	Material type	ρ [kg/m^3]	E [MPa]	ν	f_y [MPa]	Tangent E [MPa]
1	**Steel**	PIECEWISE LINEAR PLASTICITY	7850	210000	0.3	250	200

No.	Material	Material type	ρ [kg/m^3]	E [MPa]	Tension cut-off stress
2	**Mineral wool**	LOW DENSITY FOAM	100	10	0.1

No.	Material	Material type	ρ [kg/m^3]	E [MPa]	ν	f_y [MPa]	Tangent E [MPa]
3	**Seal material**	PIECEWISE LINEAR PLASTICITY	1300	10000	0.2	40	200

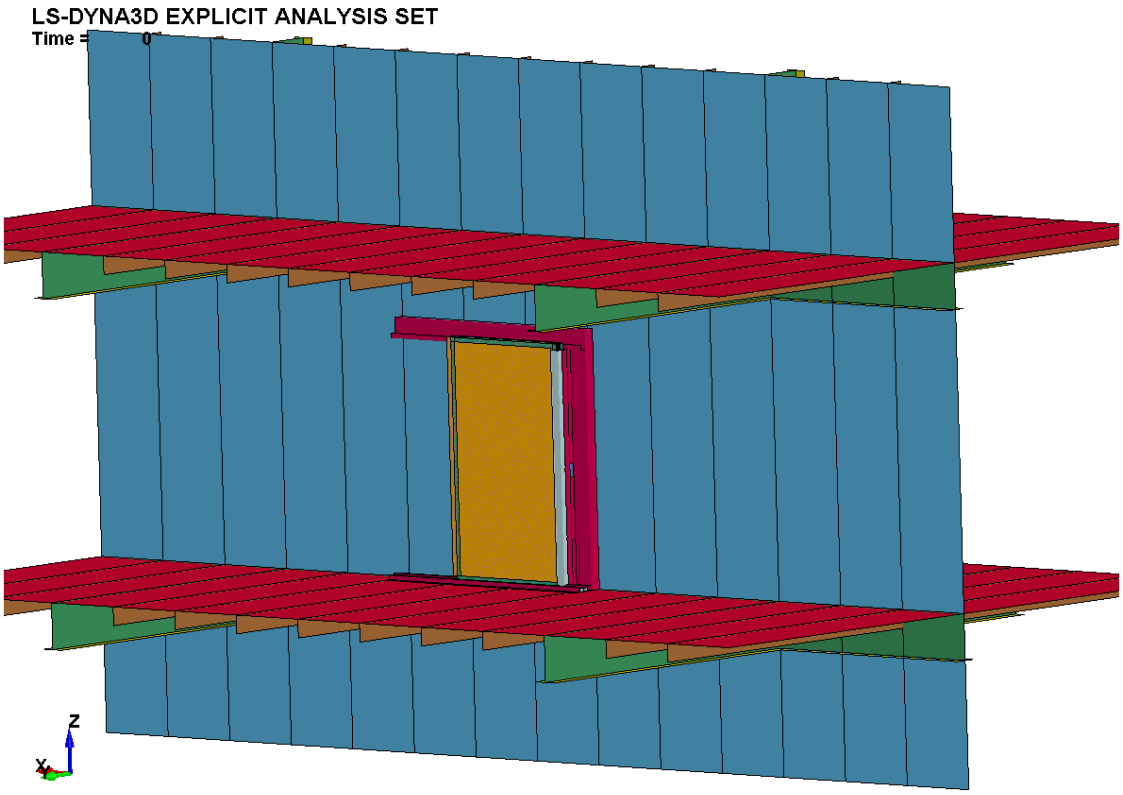

Figure 6.6.1 Initial position and boundary conditions of sliding fire-door

A hydrostatic pressure was applied from the inner side – deformed door leans on frames and rollers, not on vessel bulkhead structure. This side was chosen as presumable weaker side for loading of the SWT door. The loading scheme was similar to cold-room structure loading – first was hydrostatic pressure

applied until the upper edge of the door and in the second phase an increasing uniform load was applied to the structure until the

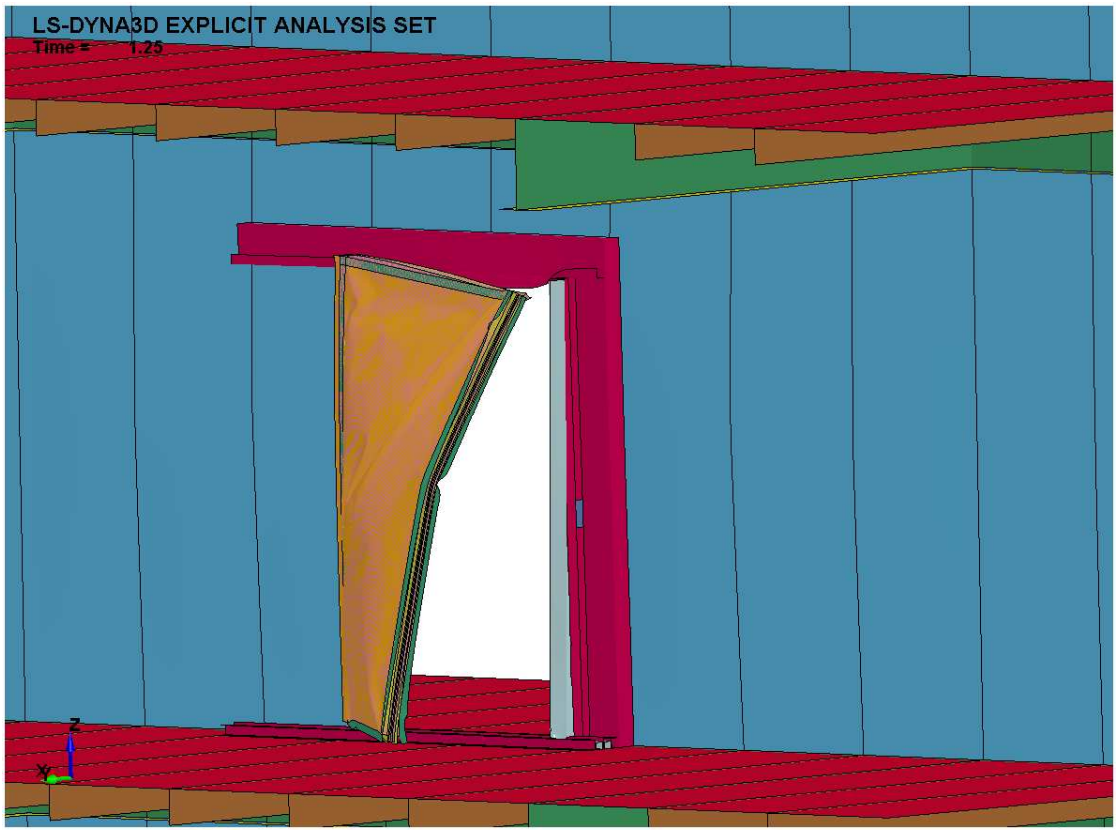

Figure 6.2 Failure of sliding door

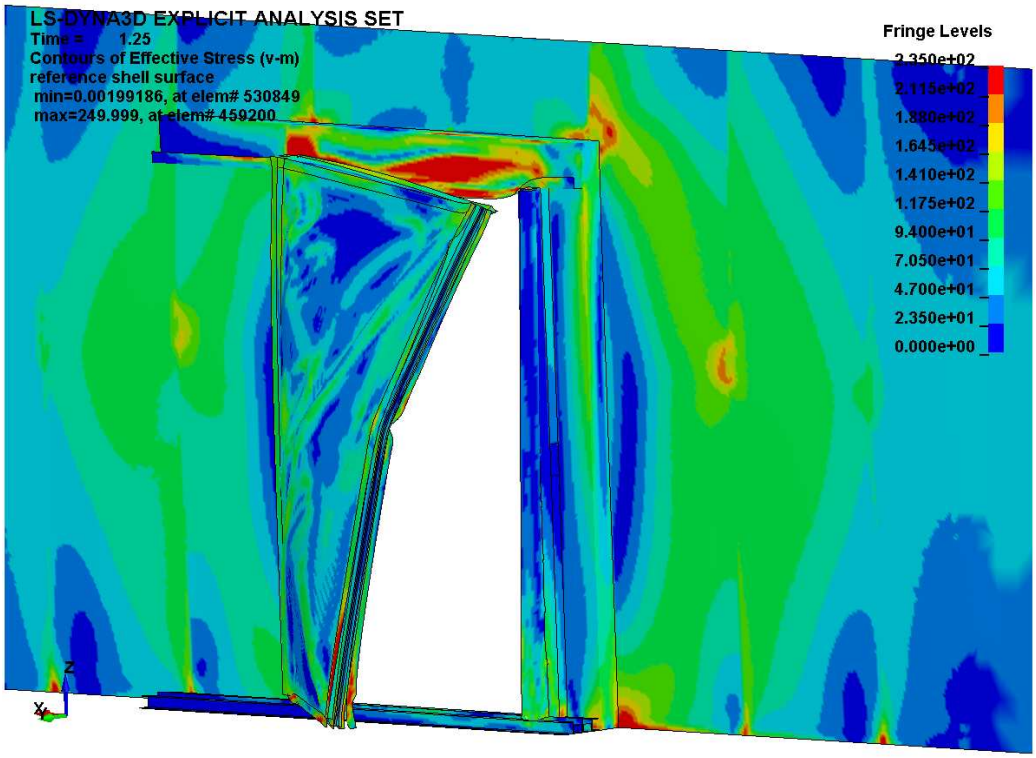

Figure 6.3 Failure of sliding door (von Mises)

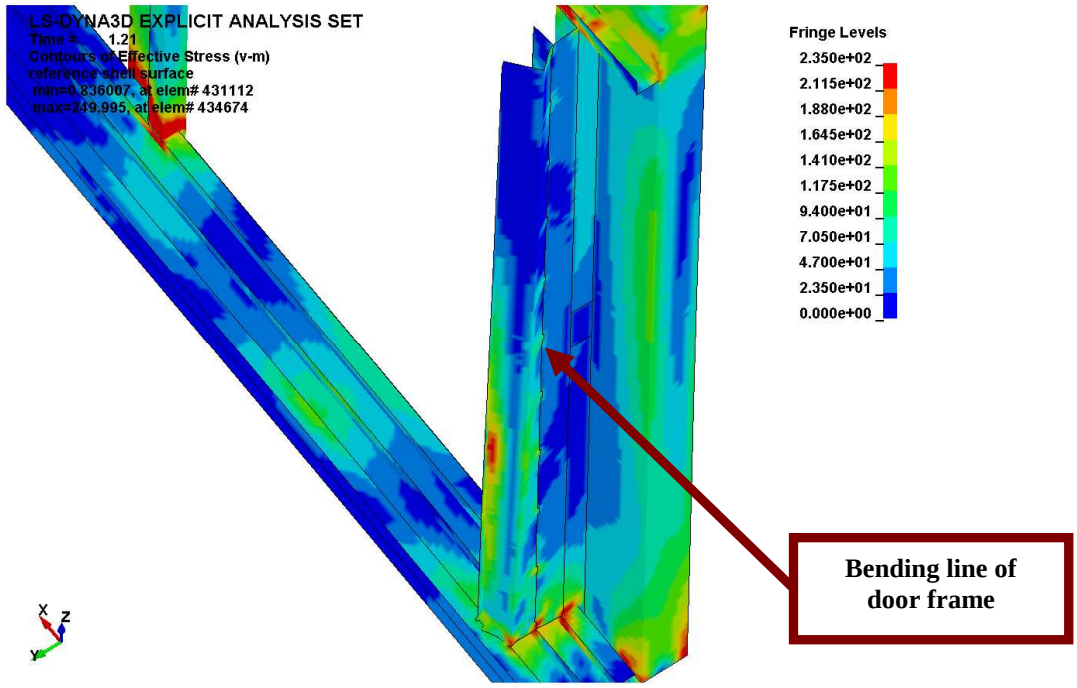

Figure 6.4 Local failure of sliding door frame

failure of structure. According to the FEM results the reason of failure was the bending of doorframe and it happened at 8.10m of hydrostatic pressure, which is equal to 79.4kPa. According to CTO results about same structure, the failure occurred at 82kPa.

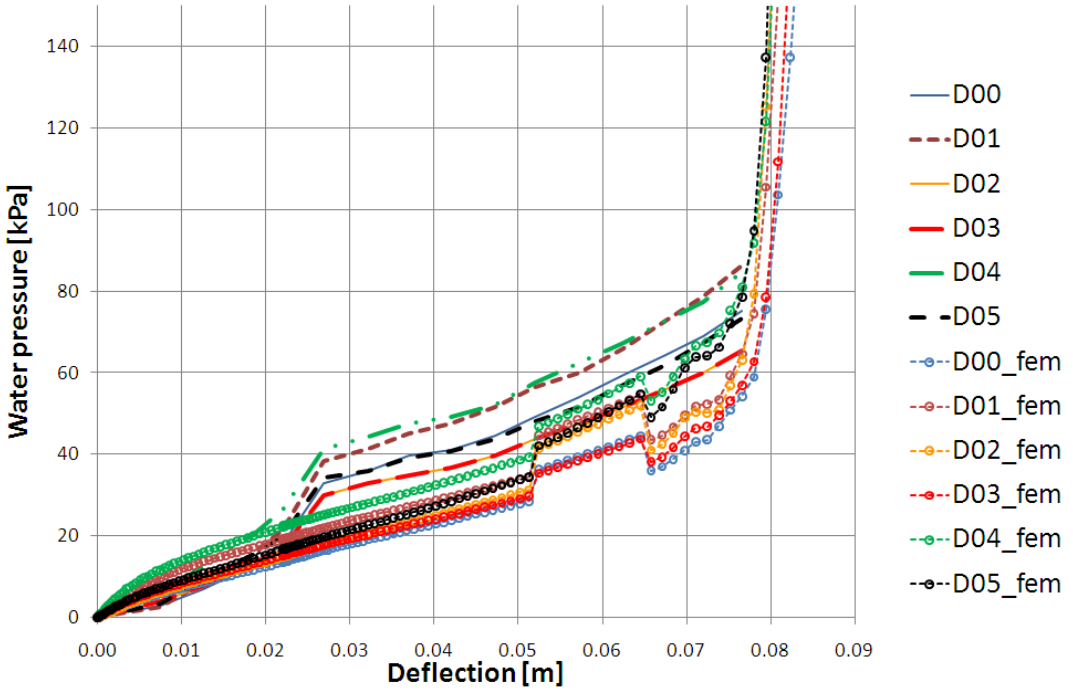

Figure 6.5 Comparison of SWT door displacement. FEM results and CTO laboratory testing

In general, the displacements of 6 different points were in quite good correlation between numerical modelling and CTO laboratory testing as seen also in figure 6.5 It must be admitted that the door closing mechanism was not modelled numerically that caused some deviation in laboratory testing.

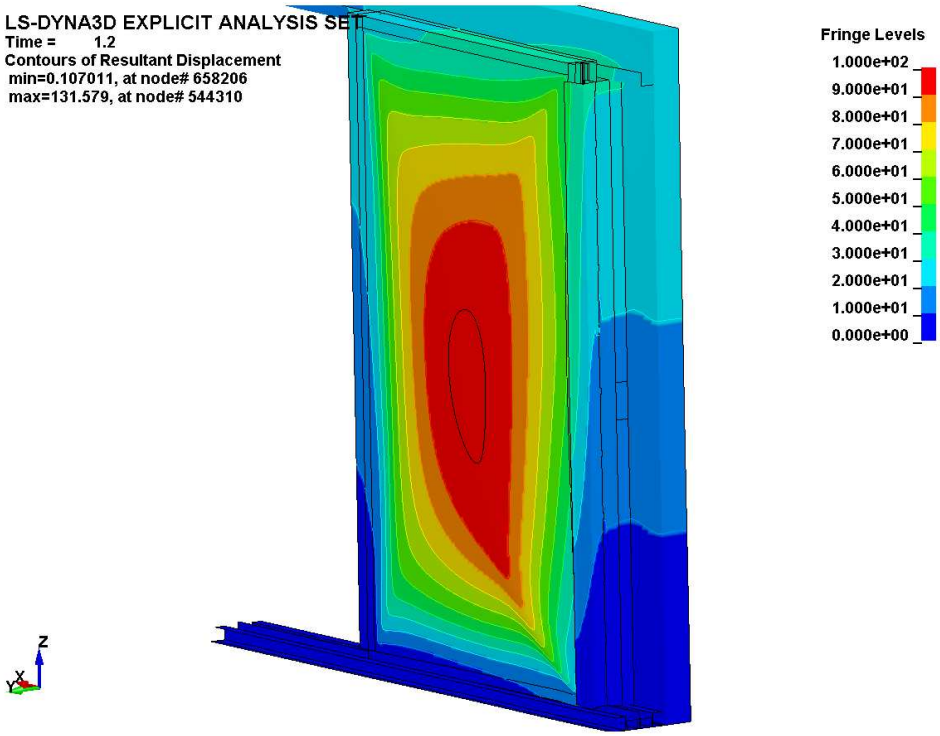

Figure 6.6 Displacement diagram of sliding door

7. COLLAPSE STRENGTH OF CABIN WALL

7.1 The procedure of estimating the strength

The study of cabin wall strength parameters were carried out similarly to cold-room wall. First, the material properties were determined by testing specimens of same cabin wall. Secondly, finite element model geometry was created according the provided panel and drawings. In finite element analysis two different models were created – a panel testing and cabin-wall model. In laboratory testing, another two tests were carried out – single panel bending test under equally distributed load (two specimens) and cabin wall leakage test under hydrostatic pressure (performed by CTO).

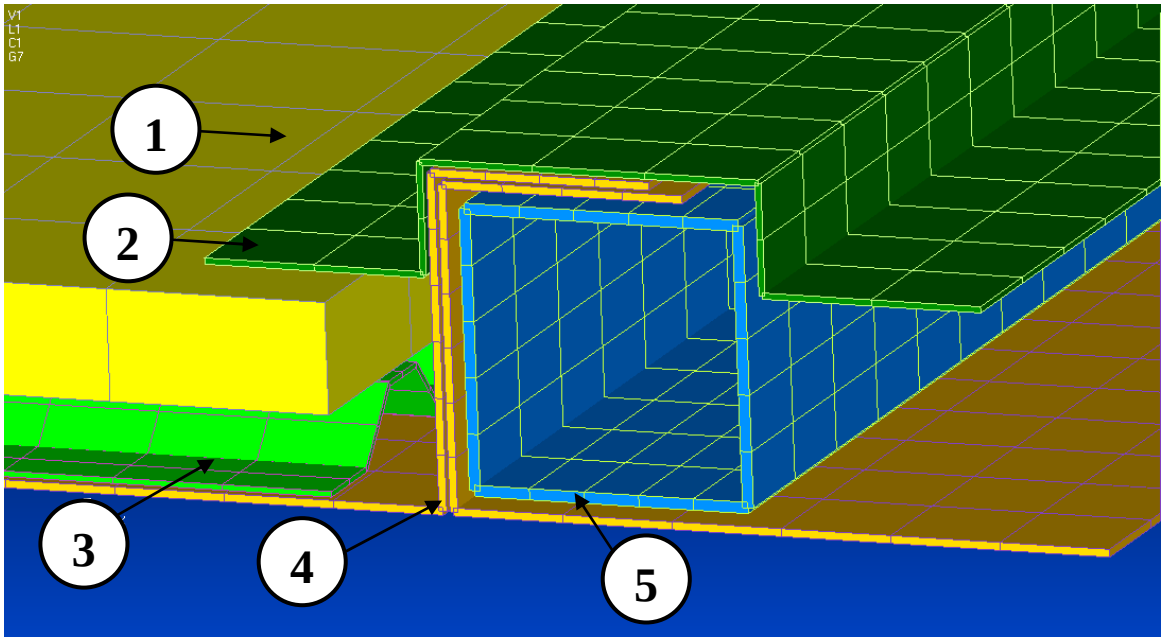

Figure 7.0.1 Cross-section of cabin-wall panel

1. Mineral wool Paroc Marine 150 slab t = 10mm
2. Galvanized Crimp Fillet (mild steel) t = 0.5mm
3. Galvanized corrugated support plate t = 0.5mm
4. PVC coated galvanized steel plate t = 0.7mm
5. Galvanized square pipe (25x25x1)

7.2 Testing of materials

Testing involved tensile test of corrugated sheet, flat galvanized steel and Paroc Marine mineral wool. The tensile tests were carried out on Zwick/Roell Z250 testing machine and mineral wool compression tests on Zwick/Roell Z2.5. Like to previous models from material testing results stress-strain curves were created to define materials in finite element model, expect for corrugated sheet. Provided

specimens were cut cross the corrugated sheet “waves” which did not let to define material stress-strain curve, but allowed to define the yield stress. Found yield stress for corrugated material was 260MPa.

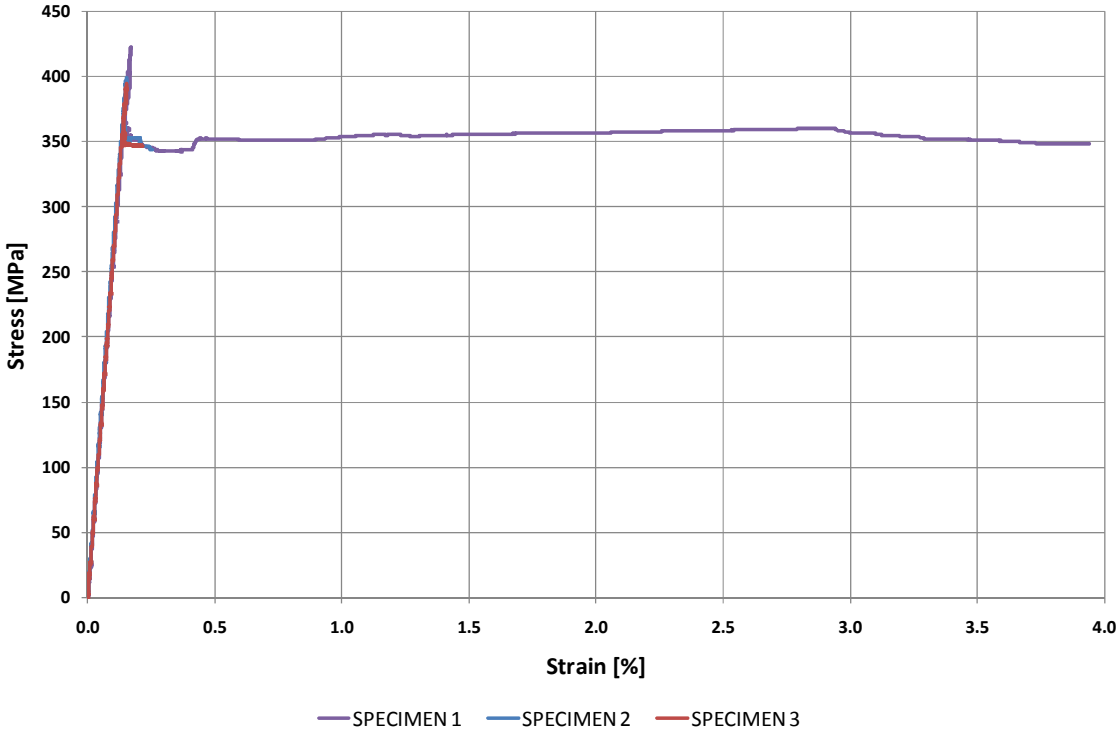

Figure 7.2 Stress-strain curve of cabin-wall flat sheet

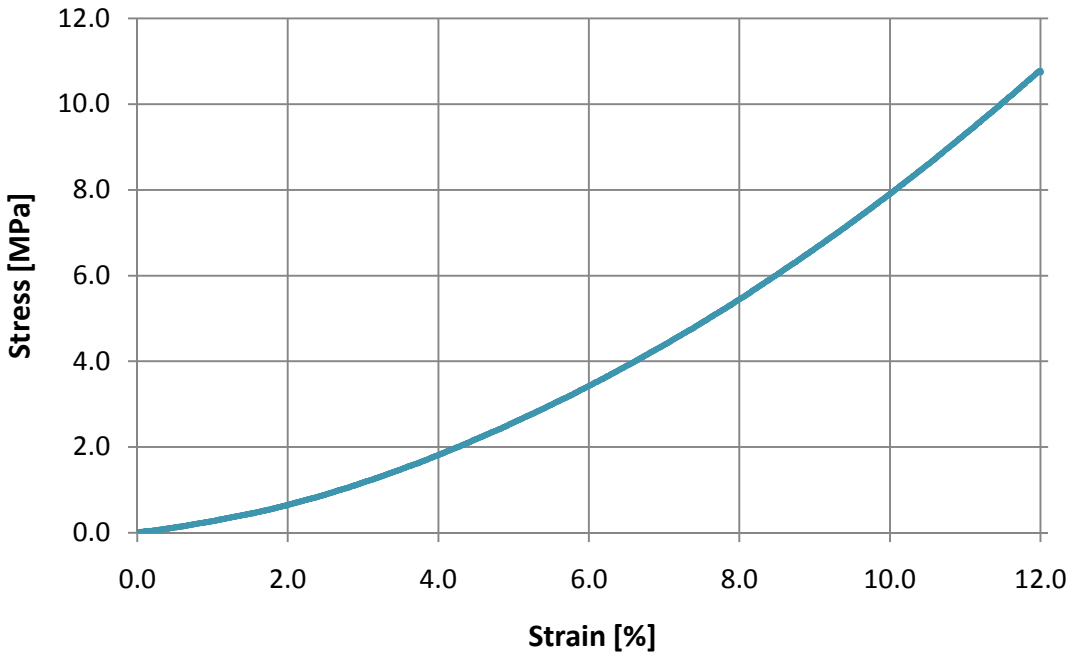

Figure 7.3 Stress-strain curve of Paroc Marine mineral wool (average)

According to material testing following material models and properties were used in FEM based LS-Dyna software:

Cabin wall materials

No.	Material	Material type	ρ [t/mm^3]	E [MPa]	Stress-strain curve included
1	**Mineral wool Paroc Marine 150 slab**	LOW DENSITY FOAM	1.50E-10	5	yes

No.	Material	Material type	ρ [t/mm^3]	E [MPa]	v	σ_y [MPa]	Tangent E [MPa]	plastic strain failure
2	**Galvanized Crimp Fillet (mild steel)**	PIECEWISE LINEAR PLASTICITY	7.85E-09	210000	0.3	260	200	0.2

No.	Material	Material type	ρ [t/mm^3]	E [MPa]	v	σ_y [MPa]	Tangent E [MPa]	plastic strain failure
3	**Galvanized corrugated support plate (mild steel)**	PIECEWISE LINEAR PLASTICITY	7.85E-09	210000	0.3	260	200	0.2

No.	Material	Material type	ρ [t/mm^3]	E [MPa]	v	σ_y [MPa]	Tangent E [MPa]	plastic strain failure
4	**PVC coated galvanized steel plate (mild steel)**	PIECEWISE LINEAR PLASTICITY	7.85E-09	210000	0.3	350	10	0.2

No.	Material	Material type	ρ [t/mm^3]	E [MPa]	v	σ_y [MPa]	Tangent E [MPa]	plastic strain failure
5	**Galvanized square pipe (mild steel)**	PIECEWISE LINEAR PLASTICITY	7.85E-09	210000	0.3	260	200	0.2

7.3 Collapse strength estimation of cabin wall panel

The strength estimation consisted of two separate procedures. Firstly, a finite element model was created and applied with line-load in the middle of the span. Secondly, a laboratory testing of panel was carried out with similar loading. In both cases, for avoiding local deformations a block of EPS was placed under loading bar.

In laboratory testing, the specimens were not identical. In original panel the wall thickness of galvanized steel square pipe was 1mm with yield stress 260N/mm^2, but in second laboratory test pipe wall thickness was 1,5mm and yield stress about 150N/mm^2 (DC01 steel). As seen in the Figure 7.4 the behaviour of original square pipes was as beam-like described in the literature. In the second laboratory test (wall 1,5mm and yield strength 150 N/mm^2) the failure of square pipes was not simultaneous. It can been also easily seen on the graph that one of the square pipes failed little earlier compared to the other.

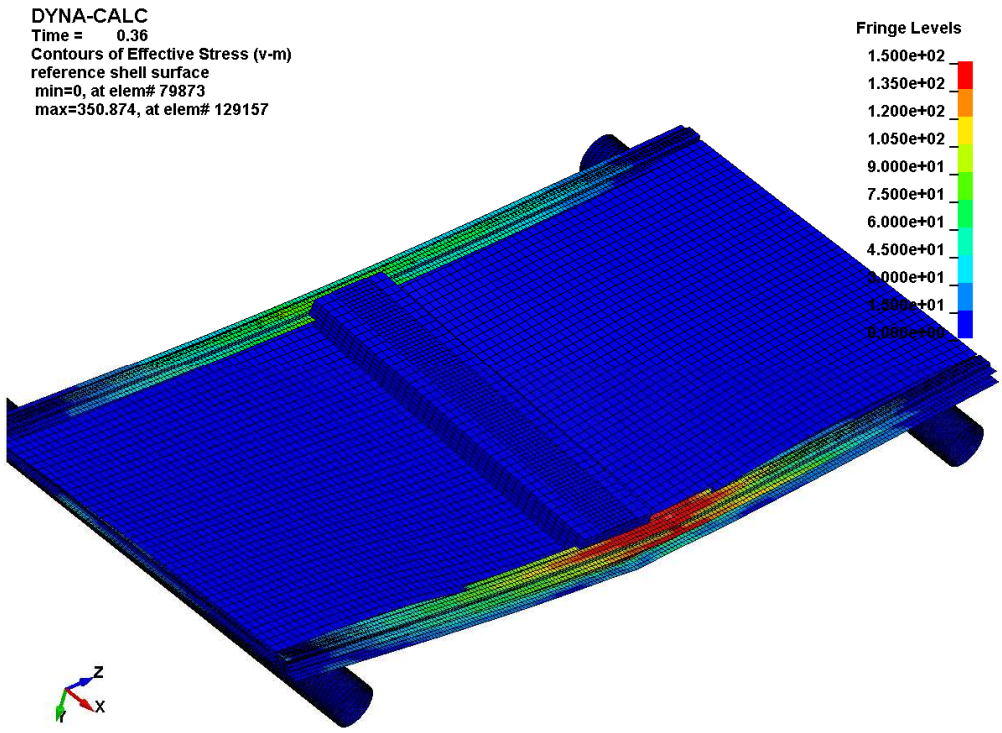

Figure 7.4 Caption of numerical modelling of cabin wall panel

FEM results were quite similar to second laboratory test, where one of the square steel pipes failed before another. The ultimate carrying capacity varied just 1,3% (F_{test} = 3147 N and F_{FEM} = 3106 N), if to consider second specimen and numerical modelling. However, if to compare the FEM results with the first specimen, the total carrying capacity differs 13.9%. The stiffness in terms of increase in carrying capacity per one mm of deflection was just 0.9% (110.96 N/mm and 109.99 N/mm) in elastic phase of the bending.

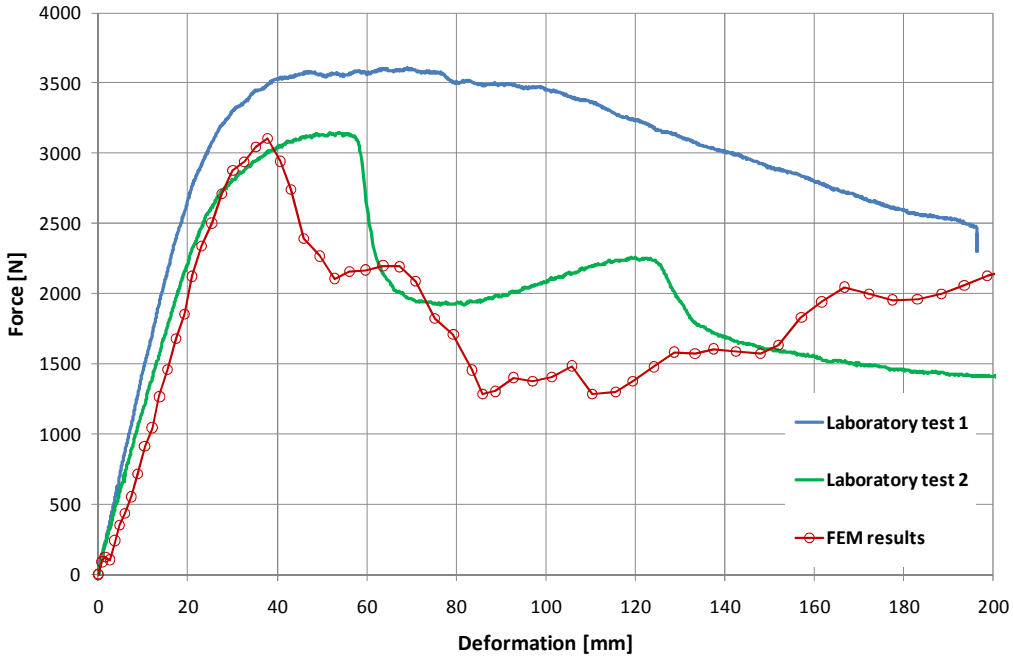

Figure 7.4 Results of cabin-wall panel testing

7.4 Collapse strength estimation of cabin wall structure

Cabin wall structure strength differs in quite large scale from single panel. If the single panel strength is determined by tubular posts and flat steel sheets screwed to it, then in cabin wall structure the strength is determined by membrane forces in wall. As the cabin wall panels are connected to each other and to vessel structure with screws – the strength of the cabin structure is determined by the strength of the screws. In the case where plain cabin wall was tested, the wall failed due failure of screws which connect panel to the floor-structure. While testing the cabin door the plain wall was again under testing because before the failure of the door, the cabin wall collapsed. In this case the strength was again determined by the screws, but not by the screws connecting to the floor, but by ones which connects two panels with each other by sides.

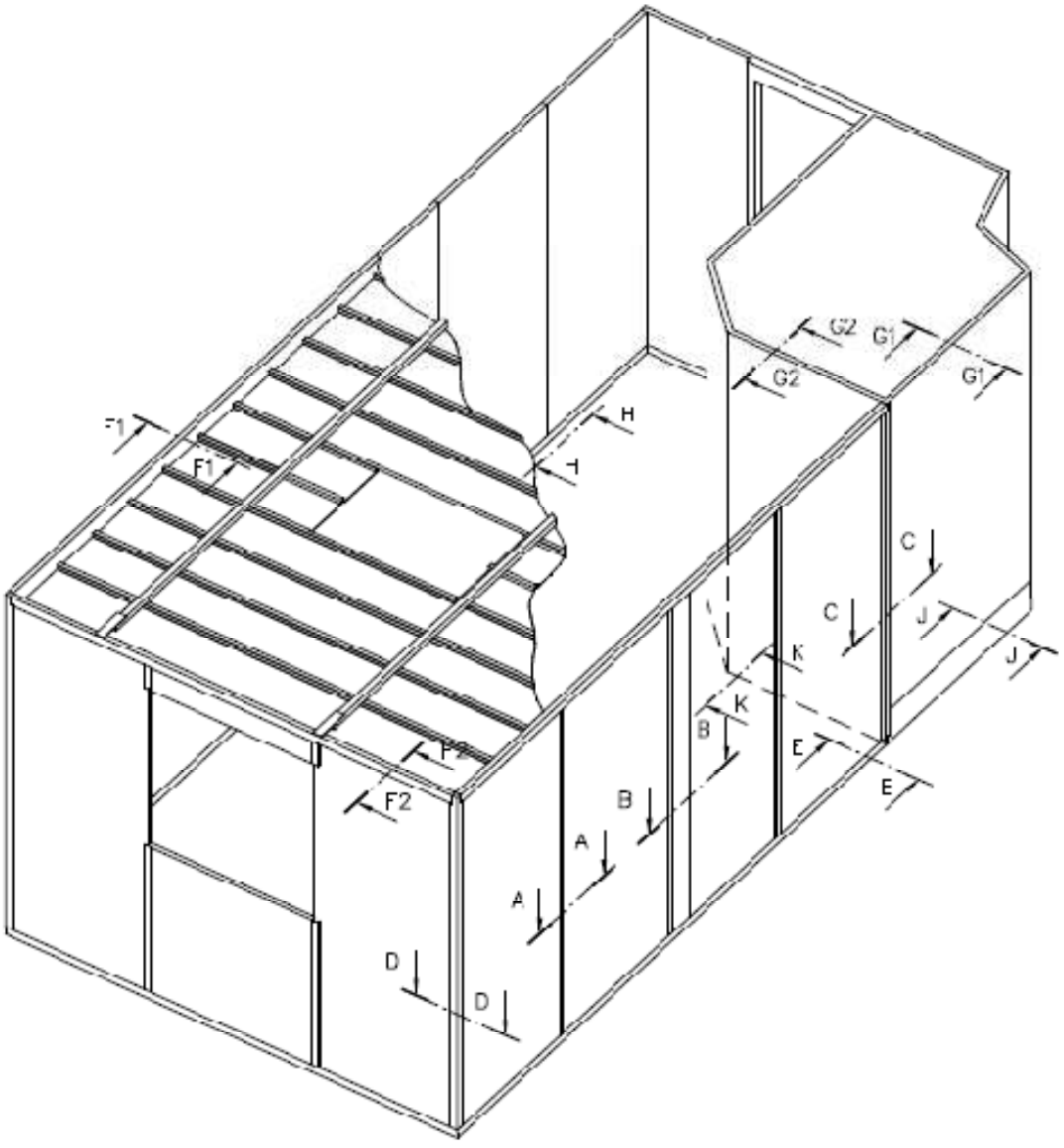

Figure 7.5 Standard cabin structure

Analytical solution for estimating the strength of cabin wall. The idea for analytical solution came by observation of laboratory test. Two main failure modes of cabin wall structure were the failure of screw joint, connecting the bottom side of a panel to the floor or failure of screw joint, connecting the panels to each other. In most cases, the failure did not mean failure of screws, but one of the connecting details – metal sheet. To determine the analytical solution for cabin wall following issues has to be considered.
Assumptions for calculations:

1. Failure occurs at the bottom between cabin wall and the deck.
2. Cabin wall panels act as individual structures (infinitely long wall)

Finding the load carrying capacity of single screw connection:
The smaller from: shear strength of screw and shear strength of one of the connecting details.

The shear strength of a self-drilling ø 4.8 screw is determined:

$$F_{v,b} = \alpha \cdot f_{u,b} \cdot A \qquad [7.1]$$

$\alpha = 0.6$

$f_{u.b} = 600\ MPa$

$A = 18.1\ mm^2$

$F_{v,b} = 0.6 \cdot 600 \cdot 18.1 = 6516\ N$

The shear strength of the thinner connecting material is determined:

$$F_{v,m} = 0.8 \cdot \alpha \cdot f_u \cdot d \cdot t \qquad [7.2]$$

$f_u = 350\ MPa$

$d = 4.8\ mm$

$t = 0.7\ mm$

$$\alpha = 3.2 \cdot \sqrt{\frac{t}{d}} = 1.22$$

$F_{v,m} = 0.8 \cdot 1.22 \cdot 350 \cdot 4.8 \cdot 0.7 = 1148\ N$

The ultimate strength depends on strength of thinner connecting detail.

Usual number of screws per one panel is 5...7 as the space between screws varies from 170mm to 230mm. It is assumed that panel is fixed with 6 screws at the bottom to the deck.
The total connection shear force capacity per panel is $6 \cdot 1148 = 6888\ N$, which in the ultimate state must be equal to reaction force of a panel at the bottom.

Next, the hydrostatic pressure for named panel reaction must be found.

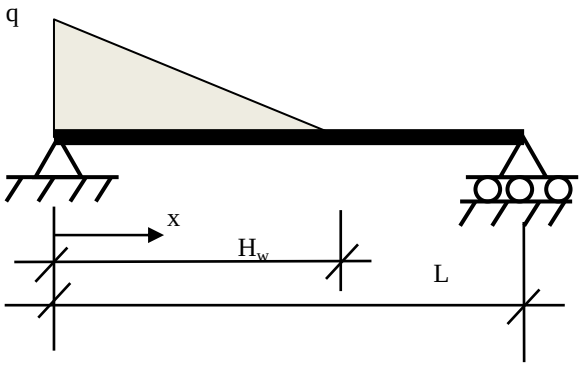

Figure 7.6 Scheme of loading and boundary conditions

Reaction force at the bottom can be found:

$$R_A = \frac{q \cdot H_w}{2 \cdot L} \cdot \left(L - \frac{H_w}{3}\right) \qquad [7.3]$$

$q = H_w \cdot b \cdot 9.81 = H_w \cdot 1200 \cdot 9.81$

if $R_A = 6888N$, then H_w must be equal to 1200 mm.

8. CRITICAL PRESSURE HEADS FOR STUDIED STRUCTURES

Following paragraph concludes the studies of structures by determining concrete pressure heads and modes for failures and gives short explanations. In single sandwich panel testing all three, FEM analyse, analytical solution and laboratory test, was carried out. First the critical bending moment of panel was calculated, secondly it was transferred to hydrostatic pressure. FEM and laboratory tests gave close results, while the analytical solution (formula no. 3.6) cave smaller pressure head as the C-shape edges were not taken into account (see table 8.1).

Sandwich panel wall FEM results and analytical solution (based on Navier solution of elastic plate, formula no. 4.1) gave similar results (see table 8.1). No laboratory test was performed because of the large scale of the test.

Laboratory test on cold-room door was limited by high leakage and FEM result rather depends on the width of whole wall, as it seems that door has higher strength compared to plain panel. No analytical solution was composed due to the complexity of the door. Instead, laboratory results should be used as the structure has standard cross-section and dimensions in most of applications. For same reasons no analytical solution for A-60 SWT door and A-60 hinged door was composed.

A-60 sliding FEM results and laboratory tests gave similar values as the ultimate strength in both cases was determined by certain element in frame (see figure 6.4).

A-60 hinged door laboratory (CTO) pressure head test was limited by large leakage as predicted and is not comparable with FEM results.

Cabin wall single panel ultimate strength was determined by bending strength while whole wall by shear force at connection to a deck.

Table 8.1 Critical pressure heads for various structures.

Analyse method / Structure	FEM analyse	Analytical solution	Laboratory test
2.0 x 7.9m sandwich panel wall	2.76 m	2.74 m	-
Single sandwich panel	3.32 m	2.67 m	3.16 m (MEC)
Cold-room door	3.86 m	-	2.40 m (CTO) (leakage limit)
A-60 SWT sliding door	8.10 m	-	8.36m (CTO)
Hinged A-60 door	2.06 m	-	0.96 (CTO) (leakage limit)
Single cabin wall panel	1.12 m	-	1.13 m (MEC)
Cabin wall 2.336 x 2.170 m (standard CTO specimen)	-	1.2 m	1.45 and 1.26 m depending on loading direction (CTO)

9. SUMMARY

This report presents numerical studies where the standard doors and lightweight walls are subjected to hydrostatic pressure. The aim was to estimate the collapse pressure for named structures and understand their behaviour. This knowledge helps to develop simplified formulas for collapse pressure estimation that can be used later on in flooding simulation.

Four types of structures were studied: cold-room structure (including wall and door), cabin wall, A-60 hinged door and A-60 semi-watertight sliding door. All these structures were analyzed with non-linear finite element method. As a result, the collapse pressure was determined. The study included also determination of material mechanical properties through testing. In order to validate the finite element results full-scale laboratory test were carried out on cold-room and cabin wall panels.

For cold room panel and for cabin wall panel the analytical models where developed in order to estimate the critical pressure heads. For standard door solutions the use of analytical methods is not practical as door failure often depends rather on the strength of joints (like screws, rivets, supporting profiles) as on the strength of the door itself.

According to results the cold room panel sustains approximately 2.7 m of water pressure. After this load the one of the face plates starts to wrinkle and collapse occurs. The cold room door sustains theoretically more load as the collapse occurs at pressure head 3.8 m. However, the CTO tests indicate that the leakage limit is reached already at 2.4 m of water height.

A-60 SWT sliding door will collapse at water height 8.1 m according to numerical simulation. The reason for the failure was the bending of doorframe. In CTO tests collapse occurred at 8.36 m of water height.

Simulation revealed that Hinged A-60 door will collapse at approximately 2 m of water level due to deformation of door joints. However, tests in CTO pointed out that the leakage limit was reached at 1 m of water level.

Tests and simulation on single cabin wall panel indicates that the panel will fail due to bending already at 1.1 m of water level. However, the panel will not collapse as at the membrane forces start carry the load. Therefore, the final failure occurs at point where the total shear force reaches to value equal to the shear strength of the panel-deck connection. According to the analytical formulas this failure will take place at water height 1.2 m. Tests done in CTO point out also that the shear failure is reason for the final damage at water level 1.2-1.4 m depending from the loading side.

Results indicate that with the proper modelling technique the collapse of partitions due to water pressure can be estimated quite well. The modelling accuracy less than 20 % compared to test results can be achieved. However, this means that very detailed models must be analysed and material properties have to be known on stress-strain curve level.

10. APPENDIXES

A.1 Design of sandwich panel testing apparatus and general set-up

A.1.1Structural design of sandwich panel testing bench

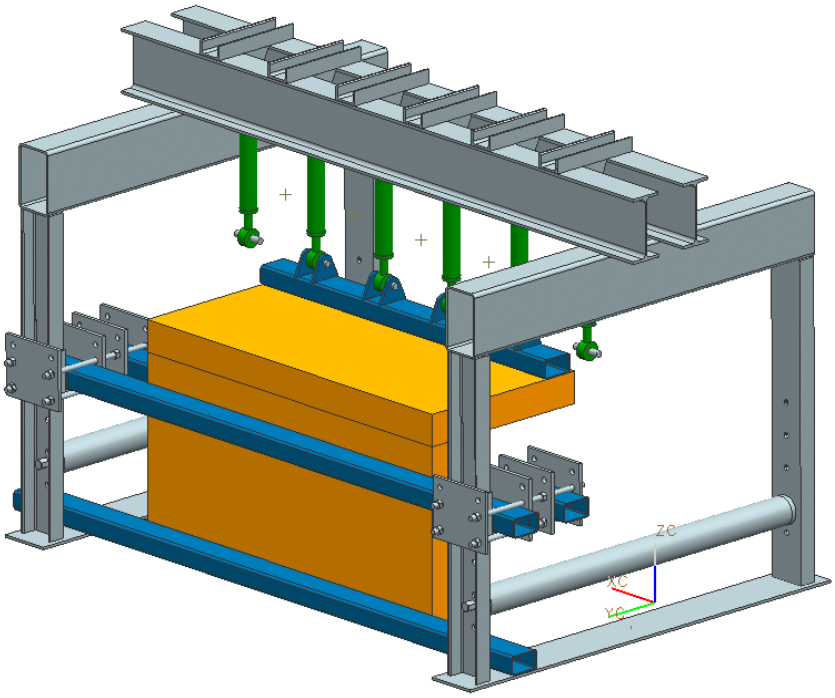

Figure 10.1: Model of sandwich panels testing apparatus (adjustment for corner element)

All bending-, locking shear-strength- and corner bending tests were carried out on bench, which was especially modified for the Floodstand project.
A three-dimensional model was created for modifications of bending apparatus for testing different shape specimens. A picture of the 3D model bending frame with different adjustments can be seen in figure 10.1 and 10.2.

Six hydraulic cylinders are used to create a uniform loading along the specimens. As sandwich panel is very likely a subject to loss of stability in a local mean, a uniform loading is essential. Uniform loading creates square parabolic bending moment along span, which indicates better the ultimate bending strength under hydrostatic pressure in a real case. The main elements (load carrying beams) of the frame were dimensioned enough rigid that results will not be affected by the deflection of the bench. To avoid even the smallest errors in the measurements, the displacement transducer was attached to isolated element.

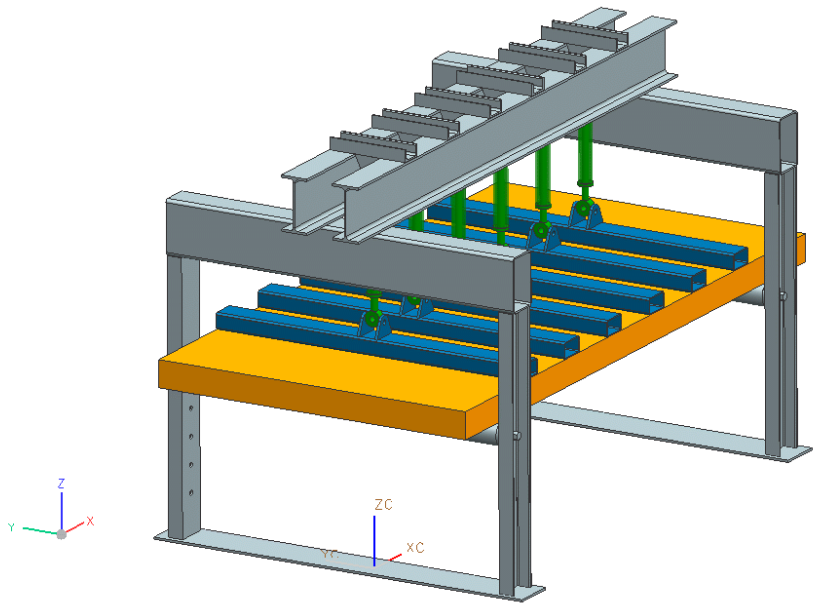

Figure 10.2: Model of sandwich panels testing apparatus (adjustment for flat element)

Loading is created by an oil pump and the access of the oil to the system is controlled by a computer-controlled valve. Cylinders are designed for up to 160 bar pressure which means that the total output of the cylinders is 120kN.

A.1.2 Calibration of bending frame

Calibration was used because it was impossible to define friction between the piston and the cylinder. Depending on the number of cylinders in use, a specific calibration was carried out.

Oil system was redesigned before the calibration because backflow oil filter caused non-linear backpressure. During the loading, filter was by-passed by backflow with special valve.

In general, two different types of calibrations were used to ensure right coefficients. First calibration was done by help of single force transducer measuring the force at one of support points. As the force transducer results could not be saved digitally, deformation extensometer was taken into use. Known standard steel beam with strain gauge was loaded by hydraulic cylinders. According to strain in the beam, a distributed load was calculated. Same procedure was repeated for several times to avoid single errors.

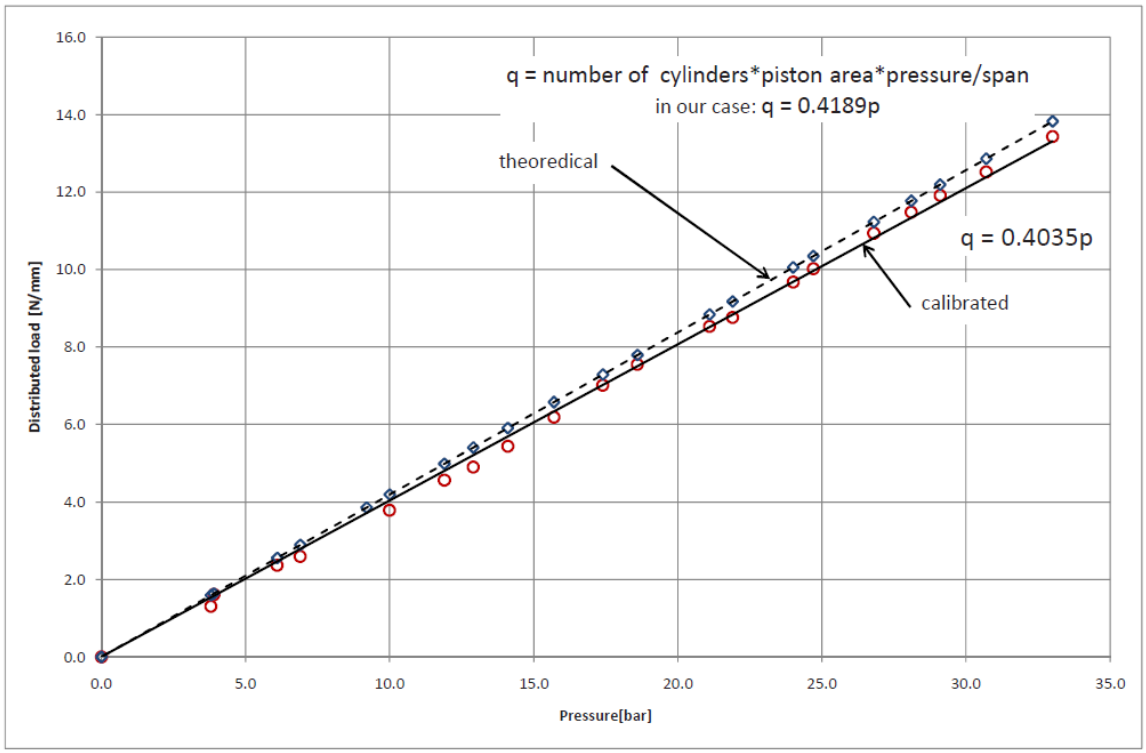

Figure 10.3: Calibration curves

Calibration curve differentiated from theoretical values quite little, which allow believing that friction in cylinders is constant and do not affect the results in large scale.

A.1.3 Testing setup

Before the setup of the test, all details (e.g beams that carry load from cylinders to a specimen) that were between the cylinders and the specimen are weighted and masses registered.

The oil pressure in the system was controlled continuously and the values of digital manometer are registered in every 0.006 seconds. The testing apparatus was equipped with a digital deflection-measuring gauge and the values were saved at same rate. These digital outputs were used for further analysis of the specimens and for the comparison of numerical calculations.

11. REFERENCES

1. Light-weight steel and aluminium structures, Fourth International Conference on Steel and Aluminium Structures, Edited by: P. Makelainen and R Hassinen

2. Facesheet Wrinkling in Sandwich Structures *Robert P. Ley, Weichuan Lin, and Uy Mbanefo Northrop Grumman Corporation, El Segundo, California, 1999,* NASA/CR-1999-208994 (pp. 8-9)

3. Mechanics of Composite Structures, Laszio P. Kollar, George S. Springer, Cambridge University Press 2003

4. Compression facing wrinkling of composite sandwich structures, E.E. Gdoutos, I.M. Daniel *, K.-A. Wang, Robert R. McCormick School of Engineering and Applied Science, Northwestern University, 327 Catalysis Building, 2137 North Sheridan Road, Evanston, IL 60208-3020, USA Received 15 June 2001; received in revised form 13 January 2002

5. Lightweight Sandwich Construction, Edited by J.M. Davies, The University of Manchester, UK, 2001 Theory and analysis of elastic plates